

Light thermal dark matter via type-I seesaw portal

Debasish Borah,^{1,*} Pritam Das,^{1,2,†} Satyabrata Mahapatra,^{3,‡} and Narendra Sahu^{4,§}

¹*Department of Physics, Indian Institute of Technology, Guwahati, Assam 781039, India*

²*Department of Physics, Salbari College, Baksa, Assam 781318, India*

³*Department of Physics and Institute of Basic Science,
Sungkyunkwan University, Suwon 16419, Korea*

⁴*Department of Physics, Indian Institute of Technology Hyderabad,
Kandi, Sangareddy 502285, Telangana, India*

Abstract

We propose a minimal scenario for light thermal dark matter (DM) in sub-GeV to GeV ballpark by incorporating a scalar singlet DM in a type-I seesaw scenario extended by an additional Higgs doublet ϕ_2 . The latter permits efficient annihilation of light scalar DM into leptonic final states including right-handed neutrinos (RHN). While DM annihilation into charged lepton final states is kept either suppressed or in a kinematically forbidden ballpark to avoid cosmic microwave background (CMB) bounds, the RHN, active neutrino final states remain safe from such bounds even if they are allowed kinematically. We discuss the interplay of forbidden and non-forbidden channels in generating light thermal DM relic while incorporating constraints from cosmology as well as laboratory experiments. The model can also explain the anomalous magnetic moment of muon, W-mass anomaly and saturate experimental bounds on charged lepton flavour violation and DM direct detection while offering tantalising detection prospects of the lightest RHN, the mass of which is kept in the same ballpark as DM.

*Electronic address: dborah@iitg.ac.in

†Electronic address: prtmDas9@gmail.com

‡Electronic address: satyabrata@g.skku.edu

§Electronic address: nsahu@phy.iith.ac.in

I. INTRODUCTION

The matter component in the present Universe is dominated by a non-luminous, non-baryonic form of matter, popularly known as dark matter (DM). This has been supported by various astrophysical observations at different scales [1–3] together with cosmological experiments like PLANCK, WMAP predicting around 26.8% of the present Universe to be made up of DM [4, 5]. In terms of density parameter Ω_{DM} and reduced Hubble parameter $h = \text{Hubble Parameter}/(100 \text{ km s}^{-1}\text{Mpc}^{-1})$, the observed DM abundance in the present epoch at 68% CL is [5]

$$\Omega_{\text{DM}}h^2 = 0.120 \pm 0.001 . \quad (1)$$

Given DM has a particle origin, none of the standard model (SM) particles can satisfy the required criteria of a particle DM. This has led to several beyond the standard model (BSM) proposals for DM out of which the weakly interacting massive particle (WIMP) has been the most popular one. In the WIMP paradigm, a DM particle having mass and interactions similar to those around the electroweak scale gives rise to the observed relic after thermal freeze-out, a remarkable coincidence often referred to as the *WIMP Miracle* [6]. A recent review of such models can be found in [7]. Typically, the interactions leading to thermal freeze-out of WIMP also give rise to sizeable DM-nucleon scattering which has been searched for at several direct detection experiments. However, no such scattering has been observed yet leading to stringent constraints on WIMP DM parameter space [8].

In view of this, light thermal DM with mass ($M_{\text{DM}} \lesssim \mathcal{O}(10 \text{ GeV})$) has received lots of attention in recent times, particularly due to weaker constraints from direct detection experiments like LZ [8]. However, it is difficult to achieve the *WIMP Miracle* in such a low mass regime typically due to insufficient annihilation rate of DM leading to thermal overproduction. For fermionic DM, the criteria of thermal DM not overclosing the Universe leads to a lower bound on its mass, around a few GeV [9, 10]. Related discussions and exceptions for scalar DM can be found in [11]. In the presence of light mediators between DM and SM sectors, however, one can achieve the correct relic abundance as pointed out in several works [12–17]¹. However, such light DM with a large annihilation rate to SM often

¹ See also Refs [18–26] where a large annihilation cross-section is achieved due to a light mediator introduced to explain DM self-interactions.

faces tight constraints from cosmic microwave background (CMB) observations [5, 27, 28]. Such constraints can be evaded if DM is kept in the kinematically forbidden regime [13, 15, 29].

Motivated by this, we consider a simple realisation of light thermal DM in a type-I seesaw framework extended by a second Higgs doublet. DM annihilates dominantly via the light neutral component of this additional Higgs doublet into light neutrinos and the lightest right-handed neutrino (RHN) of mass ranging from MeV to GeV. However, the second and third generation of RHNs can be as heavy as $\mathcal{O}(100)$ GeV. Such RHNs can take part in type-I seesaw mechanism [30–33], leading to the generation of light neutrino masses and mixing, another observed phenomenon SM fails to address. Unlike in [16] where forbidden DM mass was close to muon or tau lepton masses (also to other SM particles studied in [15]), here we can have a wide range of DM masses due to the freedom in choosing lightest RHN mass. While we keep the charged fermion final states suppressed or in kinematically forbidden mode, we check the possibility of kinematically allowing the RHN-SM neutrino final state. Due to the chosen mass of the lightest RHN in the sub-GeV to GeV ballpark, such final states do not affect the CMB spectrum significantly due to the suppressed branching ratio into charged fermions. In spite of satisfying CMB bounds on DM annihilations, the parameter space remains within the sensitivities of several direct-detection experiments. While we discuss the possibility of light scalar singlet DM in this work, it is also possible to study fermion singlet DM by introducing dimension five operators leading to DM annihilation via the neutral component of the second Higgs doublet.

Due to the existence of a light scalar component of the second Higgs doublet as well as light RHN, the model remains verifiable via heavy neutral lepton (HNL) search experiments, charged lepton flavour violation in addition to collider aspects of the second Higgs doublet. The light CP-even scalar component of the second Higgs also gives rise to a positive contribution to muon ($g - 2$) while the negative contribution from the one-loop diagram mediated by charged scalar and CP-odd scalar is tuned to be sub-dominant while being consistent with the neutrino mass and lepton flavour violation (LFV) constraints. By properly choosing the masses of the charged and CP-odd scalar while CP-even scalar is still light as per the requirement of achieving correct relic density of DM, it is also possible to explain the CDF-II W mass anomaly [34] by the self-energy correction of W-boson mass with the new doublet scalars in the loop.

This paper is organised as follows. In section II we briefly describe our model followed by a discussion of neutrino mass in section III. In section IV, we discuss the details of muon ($g - 2$) and charged lepton flavour violation followed by the discussion of CDF-II W-mass anomaly in section V. In section VI, we present the results related to light thermal DM followed by detection prospects of heavy neutral leptons in section VII. We finally conclude in section VIII.

II. THE MODEL

As we are going to discuss the possibility of light scalar singlet DM in a type-I seesaw scenario extended by a second Higgs doublet, we briefly comment upon the status of scalar singlet DM extension of the SM. In Fig. 1, we showcase the parameter space for a singlet scalar DM scenario in the plane of the singlet scalar DM coupling with SM Higgs ($\lambda S^2(\phi_1^\dagger\phi_1)$) and DM mass. The red dot-dashed line shows the contour of correct relic density considering the annihilation cross-section of S into SM fermions mediated via SM Higgs. Clearly it is difficult to achieve correct relic density below a few GeV of DM mass while being consistent with the perturbativity constraint on the coupling λ which is depicted by the purple shaded region. We also show the parameter space consistent with the most stringent constraint on DM-nucleon scattering from CRESST-III [35], DS-50 [36], XENON-nT [37] and LZ [8] depending on the DM mass with the cyan shaded region. It is evident from Fig. 1 that for DM mass below 50 GeV, there is no common parameter space that satisfies correct relic density and direct detection constraints. The coupling required to achieve sufficient annihilation cross-section so as to get the correct relic density are already ruled out by direct search experiments.

We consider a type-I seesaw model extended by a Higgs doublet (ϕ_2) and a real singlet scalar (S) with the latter being odd under an unbroken Z_2 symmetry. The singlet scalar, being stable due to Z_2 symmetry, acts like a DM candidate in the model. Thus, the scalar sector consists of the SM Higgs doublet ϕ_1 , the second Higgs doublet ϕ_2 and the Z_2 -odd scalar singlet S . In order to keep Z_2 symmetry unbroken, S does not acquire any vacuum expectation value (VEV). We consider the alignment limit of the two Higgs doublets, where only one neutral Higgs (SM-like) acquires a non-zero VEV (v) such that they can be

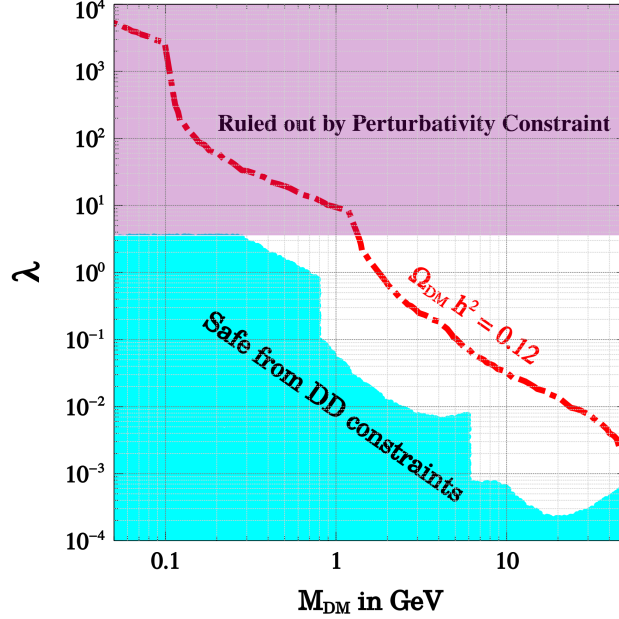


FIG. 1: Parameter space for singlet scalar DM extension of the SM in sub-GeV to GeV scale DM mass window.

parameterised as

$$\phi_1 = \begin{pmatrix} G^+ \\ \frac{1}{\sqrt{2}}(v + h_1 + iG^0) \end{pmatrix} \quad \phi_2 = \begin{pmatrix} H^+ \\ \frac{1}{\sqrt{2}}(H_2 + iA) \end{pmatrix} \quad (2)$$

The scalar potential of the model can be written as follows,

$$\begin{aligned} V = & -\mu_{\phi_1}^2 \phi_1^\dagger \phi_1 + \mu_{\phi_2}^2 \phi_2^\dagger \phi_2 + \frac{1}{2} \mu_S^2 S^2 + \frac{1}{2} \lambda_1 (\phi_1^\dagger \phi_1)^2 + \frac{1}{2} \lambda_2 (\phi_2^\dagger \phi_2)^2 + \frac{1}{4!} \lambda_3 S^4 \\ & + \lambda_3 (\phi_1^\dagger \phi_1) (\phi_2^\dagger \phi_2) + \lambda_4 (\phi_1^\dagger \phi_2) (\phi_2^\dagger \phi_1) + \frac{1}{2} \lambda_5 (\phi_1^\dagger \phi_2) (\phi_1^\dagger \phi_2) \\ & + \frac{1}{2} \lambda_{S1} (\phi_1^\dagger \phi_1) S^2 + \frac{1}{2} \lambda_{S2} (\phi_2^\dagger \phi_2) S^2 + \lambda_{HS} (\phi_2^\dagger \phi_1 + \phi_1^\dagger \phi_2) S^2. \end{aligned} \quad (3)$$

We work on the Higgs basis, where one of the neutral Higgs mass eigenstates is aligned with the direction of the VEV of the scalar field. From previous studies [38–40], it is clear that for two Higgs doublet cases, the alignment limit is independent of the choice of basis and we have considered it to be exhibited in the Higgs basis itself. The scalar doublet ϕ_1 has tree-level couplings to the SM particles. Therefore, if one of the CP-even neutral Higgs mass eigenstates is SM-like, then it must be approximately aligned with the real part of the neutral field h_1 . Hence, in the alignment limit² [38] the SM Higgs ($h_1 \sim h$) decouples

² We have considered zero mixing between these two doublets (in this case, the Z_2 basis and Higgs basis

from the new CP-even Higgs (H_2) and the mass spectrum for the physical scalars, can be obtained as follows,

$$M_h^2 = \lambda_1 v^2; \quad M_A^2 = m_{H_2}^2 - \lambda_5 v^2; \quad M_S^2 = \mu_S^2 + \lambda_{S1} v^2; \quad (4)$$

$$M_{H_2}^2 = \mu_{\phi_2}^2 + \frac{v^2}{2}(\lambda_3 + \lambda_4 + \lambda_5); \quad M_{H^\pm}^2 = M_{H_2}^2 - \frac{v^2}{2}(\lambda_4 + \lambda_5). \quad (5)$$

From the above equations, it is evident that by considering λ_4 and λ_5 of order $\mathcal{O}(1)$, it is possible to create a large mass difference between M_{H_2} and $M_{H^\pm, A}$ (in order to satisfy electroweak precision bounds [42]) and we exploit this fact to realise light forbidden DM while concurrently achieving required positive and negative contributions to anomalous magnetic moment of muon and electron respectively which is discussed in subsequent sections.

With the inclusion of three right-handed neutrinos (all are Z_2 -even), the new terms in the Yukawa Lagrangian for this model can be expressed as,

$$-\mathcal{L} \supset y_1^{\alpha k} \bar{L}_\alpha \tilde{\phi}_1 N_k + y_2^{\alpha k} \bar{L}_\alpha \tilde{\phi}_2 N_k + Y_2^\alpha \bar{L}_\alpha \phi_2 l_{R_\alpha} + \text{h.c.}, \quad (6)$$

where, $\alpha = e, \mu, \tau$ and $k = 1, 2, 3$.

The first term in the above Lagrangian gives rise to the neutrino mass generation through the type-I seesaw mechanism whereas the second term is relevant for the forbidden DM realisation with type-I seesaw portal. It is worth noting here that, this term also leads to a one-loop contribution to neutrino mass similar to the scotogenic model [43, 44]. We also consider the charged lepton Yukawa coupling with the second Higgs doublet ϕ_2 to be of diagonal type to avoid tree-level flavour changing neutral current. We are also assuming the RHN mass matrix to be diagonal for simplicity.

Our study is divided into two categories depending upon whether the second Higgs doublet ϕ_2 is neutrinophilic or leptophilic. For neutrinophilic scalar doublet ϕ_2 , only the first two terms of the interaction Lagrangian in Eq. (6) exist. In this case, the light neutrino masses are obtained by the combined contribution from the tree-level as well as the one-loop level. In the dark matter phenomenology, only the $SS \rightarrow N_1 \bar{\nu}_\alpha$ annihilation channels mediated by light H_2 dominate. However, if the ϕ_2 is assumed to be leptophilic then it can couple to charged leptons in addition to the neutrinos governed by the third term in

coincide and the quartic couplings for $(\phi_i^\dagger \phi_i) \phi_j^\dagger \phi_j$ terms will be zero [39, 41]. The Z_2 -basis corresponds to an approximate Z_2 symmetry obeyed by the scalar potential only with ϕ_2 being Z_2 -odd.

Eq. (6). This facilitates the model to explain the muon ($g - 2$) anomaly and also enhances the detection prospects at the LFV experiments like MEG, Mu3e etc. In the leptophilic scenario, DM relic density is dominantly decided by the $SS \rightarrow \ell\bar{\ell}$ channels in the forbidden ballpark. However, in the non-forbidden ballpark, $SS \rightarrow N_1\bar{\nu}_\alpha$ will dominate, as we discuss in upcoming sections. In both scenarios, we get a strong correlation between the neutrino mass, DM phenomenology and the flavour observables.

III. NEUTRINO MASS

In this setup, the mass of the active neutrino is generated through both tree-level and one-loop processes. At the tree-level, the active neutrino mass is generated through the type-I seesaw mechanism following the breaking of electroweak symmetry. On the other hand, at the one-loop level, the mass arises from the involvement of N_i and ϕ_2 particles within the loop, resembling the scotogenic origin [43, 44]. It is worth noting that, in this scenario, neither of the particles within the loop are considered potential dark matter candidates due to the absence of any exact symmetry ensuring their stability. The relevant Lagrangian for neutrino mass is given by

$$\mathcal{L} \supset -y_1^{\alpha k} \bar{L}_\alpha \tilde{\phi}_1 N_k - y_2^{\alpha k} \bar{L}_\alpha \tilde{\phi}_2 N_k - \frac{1}{2} (\bar{N}_k^c M_{N_k} N_k) + \text{h.c.} \quad (7)$$

The type-I seesaw contribution to neutrino mass is given as,

$$(m_\nu^{\alpha\beta})_{\text{tree}} = -M_D M_N^{-1} M_D^T \equiv -\frac{1}{2} y_1^{\alpha k} M_{N_k}^{-1} y_1^{k\beta} v^2; \quad (8)$$

with M_D being the Dirac mass term, which can be parameterised as $M_D = y_1 \frac{v}{\sqrt{2}}$. To ensure the connection between light neutrino oscillation parameters and the active-sterile mixing angle θ originating from type-I seesaw, we have adopted the Casas-Ibarra(CI) parameterisation in type-I seesaw [45, 46]

$$\theta_{\alpha k} = \left(i U_{\text{PMNS}} \sqrt{m_\nu^{\text{Diag}}} \mathcal{R} \sqrt{M_N^{-1}} \right)_{\alpha k} \quad (9)$$

where, U_{PMNS} is the unitary Pontecorvo-Maki-Nakagawa-Sakata leptonic mixing matrix³, m_ν^{Diag} and M_N are the 3×3 diagonal light neutrino and heavy neutrino mass matrices, respectively. Here, \mathcal{R} is an arbitrary complex orthogonal matrix, with $\mathcal{R}\mathcal{R}^T = 1$.

³ We assume the individual seesaw mass matrices to be diagonalized by the leptonic mixing matrix for simplicity. The charged lepton mass matrix is considered to be diagonal.

We also get a one-loop contribution to neutrino mass with ϕ_2 and N in the loop which is given by [44, 47]:

$$(m_\nu^{\alpha\beta})_{\text{loop}} = \sum \frac{y_2^{\alpha k} y_2^{k\beta} M_{N_k}}{32\pi^2} \left[f_k(M_{H_2}^2) - f_k(M_A^2) \right], \quad (10)$$

where, M_{N_k} is the mass eigenvalue of the RHN mass eigenstate N_k and the loop function is defined as, $f_k(M_x^2) = \frac{M_x^2}{M_x^2 - M_{N_k}^2} \ln \frac{M_x^2}{M_{N_k}^2}$. Therefore the total neutrino mass will be the sum of both tree-level and loop-level contributions, *i.e.*,

$$m_\nu^{\alpha\beta} = (m_\nu^{\alpha\beta})_{\text{tree}} + (m_\nu^{\alpha\beta})_{\text{loop}} = \sum \left[-\frac{y_1^{\alpha k} y_1^{k\beta} v^2}{2M_{N_k}} + \frac{y_2^{\alpha k} y_2^{k\beta} M_{N_k}}{32\pi^2} \left[f_k(M_{H_2}^2) - f_k(M_A^2) \right] \right]. \quad (11)$$

In our analysis, we assume equal weightage of the two contributions to the neutrino mass, *i.e.*, both the tree-level and loop-level contributions collectively account for approximately 50% of the total active light neutrino mass. We adopt a bottom-up approach in determining the neutrino mass to keep the whole analysis consistent. Initially, we use the most recent best-fit values for the neutrino parameters as per [48] to formulate the total light neutrino mass matrix. Subsequently, employing the CI parameterisation within the framework of the type-I seesaw (with a consideration of 50% contribution from tree-level neutrino masses), we derive the Yukawa couplings (y_2) governing the one-loop contribution. A more general parameterisation of the individual seesaw contributions will not drastically change the generic conclusions arrived at in our work.

IV. MUON ($g-2$) AND LFV

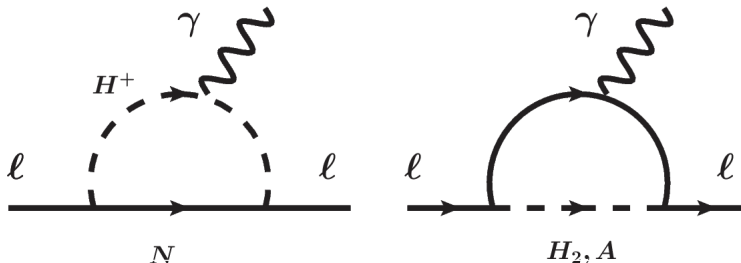


FIG. 2: One-loop diagrams contributing to the magnetic moment of leptons.

In this model, the presence of the second Higgs doublet offers the possibility to account for the anomalous magnetic moment of the muon $a_\mu = (g-2)_\mu/2$ by virtue of the loop diagrams

shown in Fig. 2. The Muon $g-2$ collaboration at the Fermilab has recently reported[49] $\Delta a_\mu = a_\mu^{\text{exp}} - a_\mu^{\text{SM}} = 249(48) \times 10^{-11}$, a discrepancy of 5.1σ CL. While recent lattice results [50] can alleviate this discrepancy to some extent, there still remains scope for BSM physics to play the leading role in explaining this discrepancy [51–53].

The new contributions to $(g-2)_\mu$ with the neutral scalars in the loop is given by[52]

$$\Delta a_\mu(H_2) = \frac{1}{8\pi^2} \frac{m_\mu^2}{M_{H_2}^2} \int_0^1 dx \frac{(Y_2^\mu)^2 x^2(2-x)}{(1-x)(1-x\left(\frac{m_\mu}{M_{H_2}}\right)^2) + x\left(\frac{m_\mu}{M_{H_2}}\right)^2} \quad (12a)$$

$$\Delta a_\mu(A) = -\frac{1}{8\pi^2} \frac{m_\mu^2}{M_A^2} \int_0^1 dx \frac{(Y_2^\mu)^2 (x^3)}{(1-x)(1-x\left(\frac{m_\mu}{M_A}\right)^2) + x\left(\frac{m_\mu}{M_A}\right)^2} \quad (12b)$$

and the contribution from the charged scalar and RHN loop is given by

$$\Delta a_\mu(H^+) = -\frac{1}{8\pi^2} \frac{m_\mu^2}{M_{H^+}^2} \int_0^1 dx \sum_k \frac{|y_2^{\mu k}|^2 2x^2(1-x)}{\left(\frac{M_{N_k}^2}{M_{H^+}^2}\right) (1-x) \left(1 - \left(\frac{m_\mu}{M_{N_k}}\right) x\right) + x}. \quad (13)$$

Here, we observe three novel contributions from BSM physics affecting the muon anomalous magnetic moment, stemming from one-loop diagrams involving H_2 , A , and H^+ particles in the loop. The contribution originating from the H_2 loop yields a positive contribution, whereas those involving A and H^+ yield negative impacts. Given the muon anomalous magnetic moment being reportedly positive, precise tuning of the masses of H_2 , A , and H^+ and their corresponding couplings is required to yield an overall positive Δa_μ . Clearly, to achieve the accurate Δa_μ , it is imperative for the contribution from H_2 to surpass that of A and H^+ .

The same particles in the loop can also contribute to LFV decays like $\mu \rightarrow e\gamma$. Since we have assumed charged lepton coupling with ϕ_2 to be diagonal, we get the significant new physics contributions only from the charged scalar and RHN loop. The branching ratio for the $\mu \rightarrow e\gamma$ process mediated via the charged scalar can be estimated as [52]

$$\text{BR}(\mu \rightarrow e\gamma) \approx \frac{3(4\pi)^3 \alpha_{\text{em}}}{4G_F^2} (|A_{e\mu}^M|^2 + |A_{e\mu}^E|^2), \quad (14)$$

where the form factors are defined as follows

$$A_{e\mu}^M = \frac{-1}{(4\pi)^2} \sum_k \left[y_2^{ke*} y_2^{k\mu} (G^+ + G^-) \right], \quad (15a)$$

$$A_{e\mu}^E = \frac{i}{(4\pi)^2} \sum_k \left[y_2^{ke*} y_2^{k\mu} (G^+ + G^-) \right], \quad (15b)$$

with the loop function being

$$G^\pm \simeq \frac{1}{M_{H^+}^2} \int_0^1 dx \int_0^1 dy x(1-x) \frac{xy \pm \left(\frac{M_{N_k}}{m_\mu}\right)}{\left(\frac{M_{N_k}^2}{M_{H^+}^2}\right) (1-x) \left(1 - \left(\frac{m_\mu^2}{M_{N_k}^2}\right) xy\right) + x}. \quad (16)$$

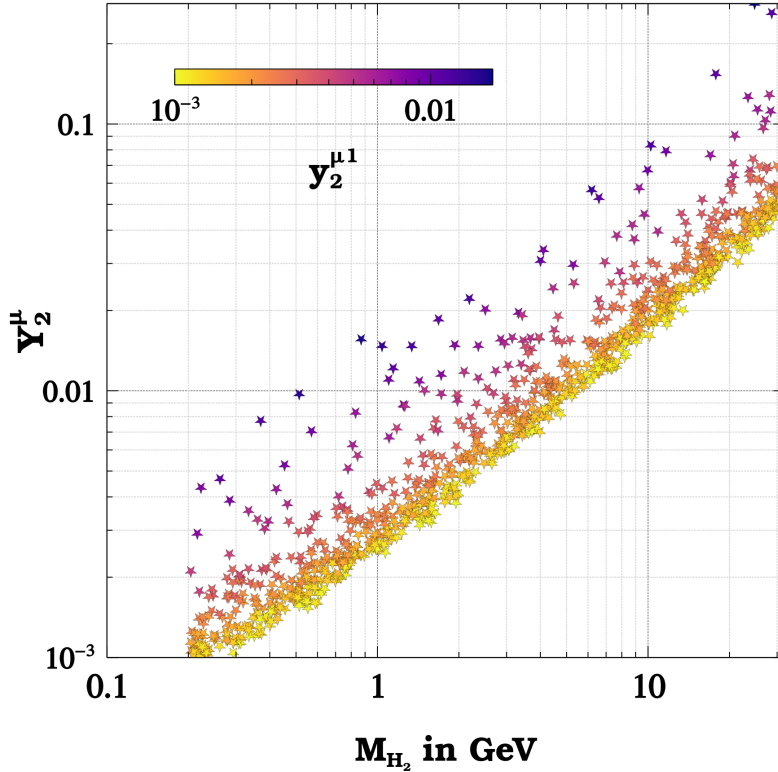


FIG. 3: Parameter space giving rise to correct Δa_μ consistent with the most recent constraint on $\text{BR}(\mu \rightarrow e\gamma)$ from MEG-II [54]

In Eq. (14), G_F is the Fermi constant and α_{em} is the fine-structure constant. From the experimental point of view, the current upper limits on the $\mu \rightarrow e\gamma$ branching ratio from MEG-2016 result is $\text{BR}(\mu \rightarrow e\gamma) < 4.2 \times 10^{-13}$ [55], with future sensitivity being $\text{BR}(\mu \rightarrow e\gamma) < 6 \times 10^{-14}$ [56]. Fig. 3 shows the parameter space in terms of Yukawa couplings of the muon with ϕ_2 and light neutral CP-even scalar mass which can explain the anomalous muon ($g - 2$) while being consistent with the MEG upper limits on $\mu \rightarrow e\gamma$. The Yukawa coupling of the muon with the charged scalar and RHN is shown in the colour code. Since H_2 mass is smaller as compared to A and H^+ , it is possible to achieve correct Δa_μ through the one-loop diagram involving H_2 while the negative contribution from H^+ and A loop remains suppressed. In the numerical scan, we randomly vary M_{H_2} within the

range of $[0.2, 30]$ GeV, and set M_A to be approximately equal to M_{H^+} within the interval of $[100, 200]$ GeV, while ensuring the perturbativity of the scalar couplings. The mass of RHNs is varied such that $M_{N_1} > 2M_{DM}$. (*i.e.* $M_{N_1} = 2M_{DM}(1 + \Delta)$ with $\Delta \in [0.001, 1]$) and $M_{N_2} = M_{N_3} = M_{N_1} + 100$ GeV. The reason behind such a choice will be clear when we discuss the forbidden DM scenario in subsequent sections.

V. W-MASS ANOMALY

In our scenario, a positive contribution to the ρ parameter can come from the self-energy correction of the W-boson with the new doublet scalar. This additional contribution to self-energy correction $\Delta\rho$ and hence the T -parameter ($= \Delta\rho/\alpha_{\text{em}}$) is given by [57, 58]:

$$T = \frac{\Theta(M_{H^+}^2, M_{H_2}^2) + \Theta(M_{H^+}^2, M_A^2) - \Theta(M_{H_2}^2, M_A^2)}{16\pi^2\alpha_{\text{em}}(M_Z)v^2}, \quad (17)$$

with the loop function Θ given by:

$$\Theta(x, y) \equiv \frac{1}{2}(x + y) - \frac{xy}{x - y} \ln\left(\frac{x}{y}\right). \quad (18)$$

In addition to the T -parameter contribution, the S -parameter can also modify the W -boson mass slightly. The S parameter is given as,

$$S = \frac{1}{12\pi} \log\left[\frac{M_{H_2}^2 + M_A^2}{2M_{H^+}^2}\right]. \quad (19)$$

The modified W -boson mass considering both these contributions is given by [59, 60]

$$M_W \simeq M_W^{SM} \left[1 - \frac{\alpha_{\text{em}}(M_Z)(S - 2 \cos^2 \theta_W T)}{4(\cos^2 \theta_W - \sin^2 \theta_W)} \right]. \quad (20)$$

We observe that the alteration in the W -boson mass caused by the S parameter is generally negligible, with the primary correction arising dominantly from the T parameter. In Fig. 4, we showcase the parameter space in the plane of M_A and $(M_{H^+} - M_A)$ with $(M_A - M_{H_2})$ depicted in the color code. Note that all these points also satisfy the correct muon $(g-2)$ as well as is consistent with the constraints from LFV experiments as discussed in the section IV. Clearly it is possible to explain the CDF-II W -mass anomaly [34] with $M_{H_2} \in [0.2, 30]$ GeV and $M_A \in [100, 200]$ GeV while $M_{H^+} \in M_A + [40, 70]$ GeV.

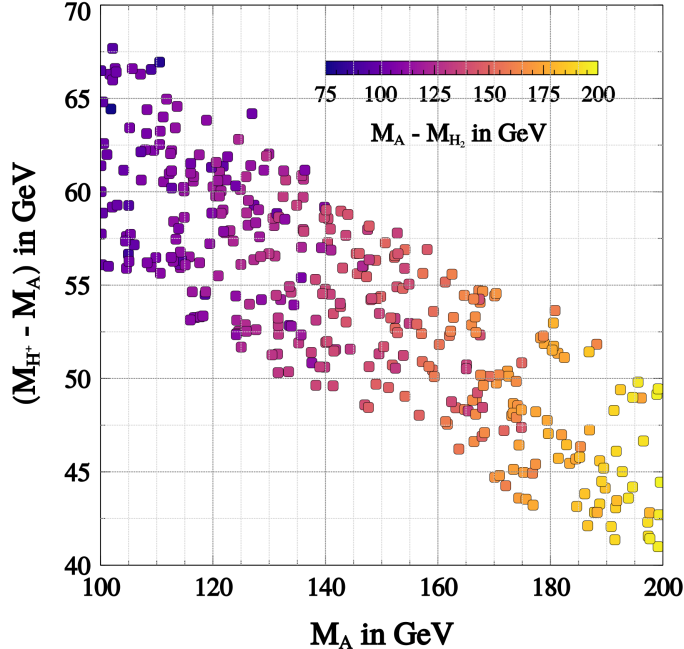


FIG. 4: Parameter space in the plane of doublet scalar masses that can explain CDF-II W-mass anomaly while being consistent with the muon $(g - 2)$ and LFV constraints.

VI. LIGHT THERMAL DARK MATTER

While the WIMP paradigm is straightforward [6], in kinematically forbidden DM scenarios [13, 15, 29], the mass of the final-state particles to which DM annihilates into in the early Universe exceeds that of the initial state or DM particles. This is made feasible by fixing a small mass difference between the initial and final-state particles, thereby introducing the essential Boltzmann suppression factor required to achieve the appropriate dark matter relic abundance. Such forbidden DM freezes out earlier compared to standard thermal WIMP DM due to Boltzmann suppression associated with heavier final states at lower temperatures. One can still satisfy the correct relic by resonantly enhancing the annihilation channels in the forbidden regime. We consider this possibility in our model where light-forbidden DM S , annihilates via light mediator (a neutral component of second scalar doublet ϕ_2) into different final states depending upon neutrinophilic or leptophilic nature of ϕ_2 . We discuss these two sub-cases separately in this section.

A. The neutrinophilic ϕ_2

The forbidden channels governing the relic abundance of dark matter in this scenario involve the process $SS \rightarrow N_1 \bar{\nu}_\alpha$ mediated by H_2 where N_1 is the lightest RHN. Given the negligible mass of the SM neutrinos (ν_α) in comparison to both S and N_1 , the relative mass difference between the initial and final state particles can be parameterised as $\Delta = (M_{N_1} - 2M_{\text{DM}})/2M_{\text{DM}}$. We explore the light mass region of dark matter ranging from 50 MeV to 5 GeV where either getting the correct relic of thermal WIMP is difficult or CMB bounds exclude such light DM annihilating into SM charged fermions during recombination. Since DM annihilates primarily into N_1 and neutrinos, one can keep DM in a kinematically forbidden ballpark by suitably adjusting the mass of N_1 . However, we can not take arbitrarily light N_1 as its late decay into SM particles may be in conflict with cosmology. In fact, there exists a lower limit on the HNL mass, derived from big bang nucleosynthesis, which stipulates that if the HNL mass falls below 100 MeV, it can potentially disrupt the successful predictions of BBN [61, 62]. This lower bound on HNL mass justifies the choice of the lower bound on DM mass considered in our analysis.

The evolution of DM number density (n_{DM}) in the early Universe is obtained by solving the Boltzmann equation incorporating the number-changing processes as,

$$\frac{dn_{\text{DM}}}{dt} = -3\mathcal{H}n_{\text{DM}} - \langle\sigma v\rangle_{SS \rightarrow N_1 \bar{\nu}_\alpha} (n_{\text{DM}}^2 - (n_{\text{DM}}^{\text{eq}})^2), \quad (21)$$

where, \mathcal{H} is the Hubble expansion rate of the Universe and $n_{\text{DM}}^{\text{eq}}$ is the equilibrium DM number density. One can also express the same equation in terms of the co-moving number density (Y_{DM}) by dividing the DM number density with the entropy density (s), *i.e.*, $Y_{\text{DM}} = n_{\text{DM}}/s$. The cross-section for the $SS \rightarrow N_1 \bar{\nu}_\alpha$ process is

$$\sigma(SS \rightarrow N_1 \bar{\nu}_\alpha) = \frac{v^2 y_2^2 \lambda_{HS}^2 (s - M_{N_1}^2)}{32\pi (s - M_{H_2}^2) (s - 4M_S^2)} \sqrt{\frac{s - 4M_S^2}{s^3}}, \quad (22)$$

where, $y_2 = \sqrt{\sum_\alpha |y_2^{\alpha 1}|^2}$.

The standard approach to solving the Boltzmann equation (BE) involves calculating the annihilation cross-section for the process $SS \rightarrow N_1 \bar{\nu}_\alpha$ and solving it numerically. However, in the case of forbidden dark matter, where the final state particles are slightly heavier than the initial states, these forward cross-sections are kinematically disallowed. For the annihilation process in thermal equilibrium, we have $(n_{\text{DM}}^{\text{eq}})^2 \langle\sigma v\rangle_{SS \rightarrow N_1 \bar{\nu}_\alpha} = (n_{N_1}^{\text{eq}})^2 \langle\sigma v\rangle_{N_1 \bar{\nu}_\alpha \rightarrow SS}$, leading to

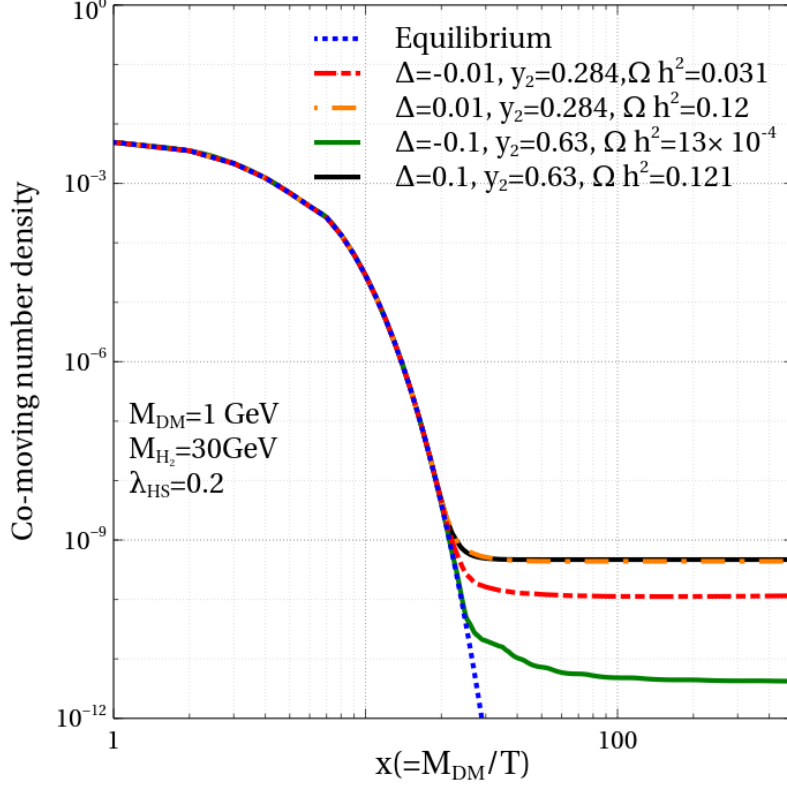


FIG. 5: Evolution of comoving abundance of DM for different benchmark choices of couplings and mass differences, showing the difference between forbidden DM and usual thermal DM freeze-out.

$\langle\sigma v\rangle_{SS\rightarrow N_1\bar{\nu}_\alpha} \simeq \langle\sigma v\rangle_{N_1\bar{\nu}_\alpha\rightarrow SS} \times e^{-2\Delta x}$ where $x = M_{\text{DM}}/T$. Using this approach, we develop our own Mathematica v13.1 code while also verifying the results using `micrOmegas` v5.3.35 [63].

We selected specific benchmark values for the free parameters in the analysis of dark matter. The mass of H_2 is chosen between 5 GeV and 30 GeV. We also choose the charged scalar (H^+) and pseudoscalar (A) masses as $M_A = M_{H^\pm} = 150$ GeV, which remain consistent with collider bounds. The other two neutral lepton masses are assumed to be much heavier than N_1 (*i.e.* $M_{N_2} = M_{N_3} = M_{N_1} + 100$ GeV) and hence they remain decoupled from generating DM relic. Fig. 5 shows the evolution of the comoving number density of DM ($Y_{\text{DM}} = n_{\text{DM}}/s$). Clearly, the freeze-out occurs earlier for a larger Δ due to the Boltzmann suppression at lower temperatures. For comparison, we also show the evolution with $\Delta < 0$, which corresponds to ordinary thermal DM where annihilation to final states is kinematically allowed. Fig. 6 shows the DM relic satisfied contours with $\Omega h^2 = 0.12$ in y_2 and M_{DM} plane. The dip in the values of Yukawa coupling around certain DM mass is due to the resonance

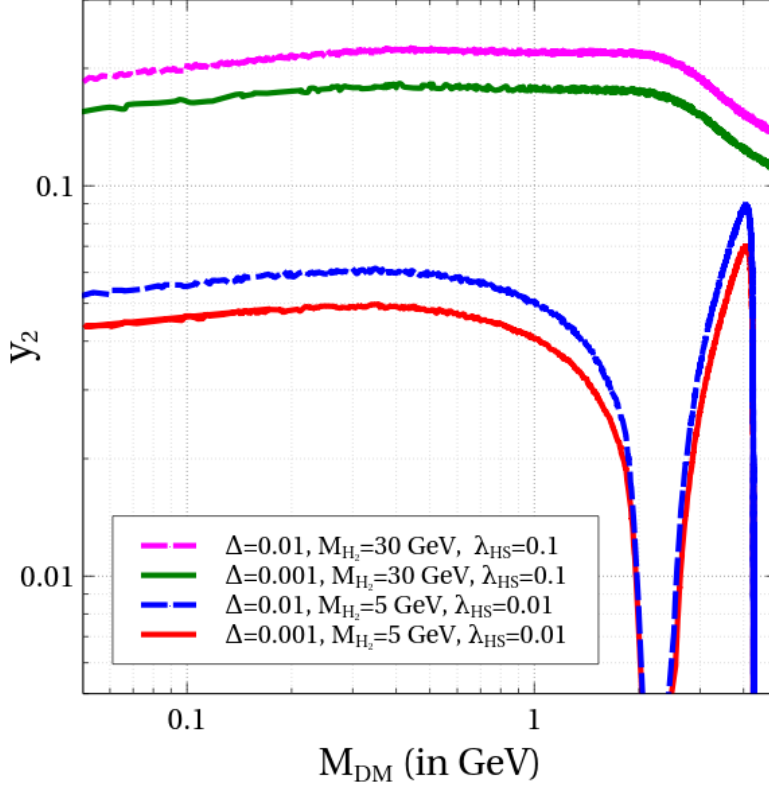


FIG. 6: Contour lines stand for $\Omega h^2 = 0.12$ in the Yukawa (y_2) *vs.* dark matter mass with two benchmark mediator values M_{H_2} , two mass splitting with fixed Higgs portal coupling. Tiny Yukawa pulls the allowed parameter space towards the s -channel resonance region for a smaller mediator mass.

effect where $M_{\text{DM}} \sim M_{H_2}/2$. The upper pink and green contours correspond to larger mediator mass ($M_{H_2} = 30$ GeV), whereas the red and blue contours correspond to smaller mediator mass ($M_{H_2} = 5$ GeV). The dashed contours stand for $\Delta = 0.01$ while the solid contours stand for $\Delta = 0.001$.

Fig. 7 shows the parameter space in y_2 and λ_{HS} plane satisfying DM relic for different combinations of Δ and M_{DM} . We can see that larger values of Δ , with other parameters fixed, require larger Yukawa coupling to get the correct relic. This is needed in order to overcome the strong Boltzmann suppression brought in by a larger value of Δ . The correlation between λ_{HS} and y_2 in Fig. 7 can be understood as $\langle\sigma v\rangle \propto \lambda_{HS}^2 y_2^2$. For a fixed DM mass and mass-splitting, as we decrease $|\lambda_{HS}|$, $\langle\sigma v\rangle$ decreases which overproduce the DM and hence y_2 has to be increased to achieve the correct relic density. It should be noted that, while DM annihilation to $N_1 \bar{\nu}_\alpha$ can be kept in kinematically forbidden mode

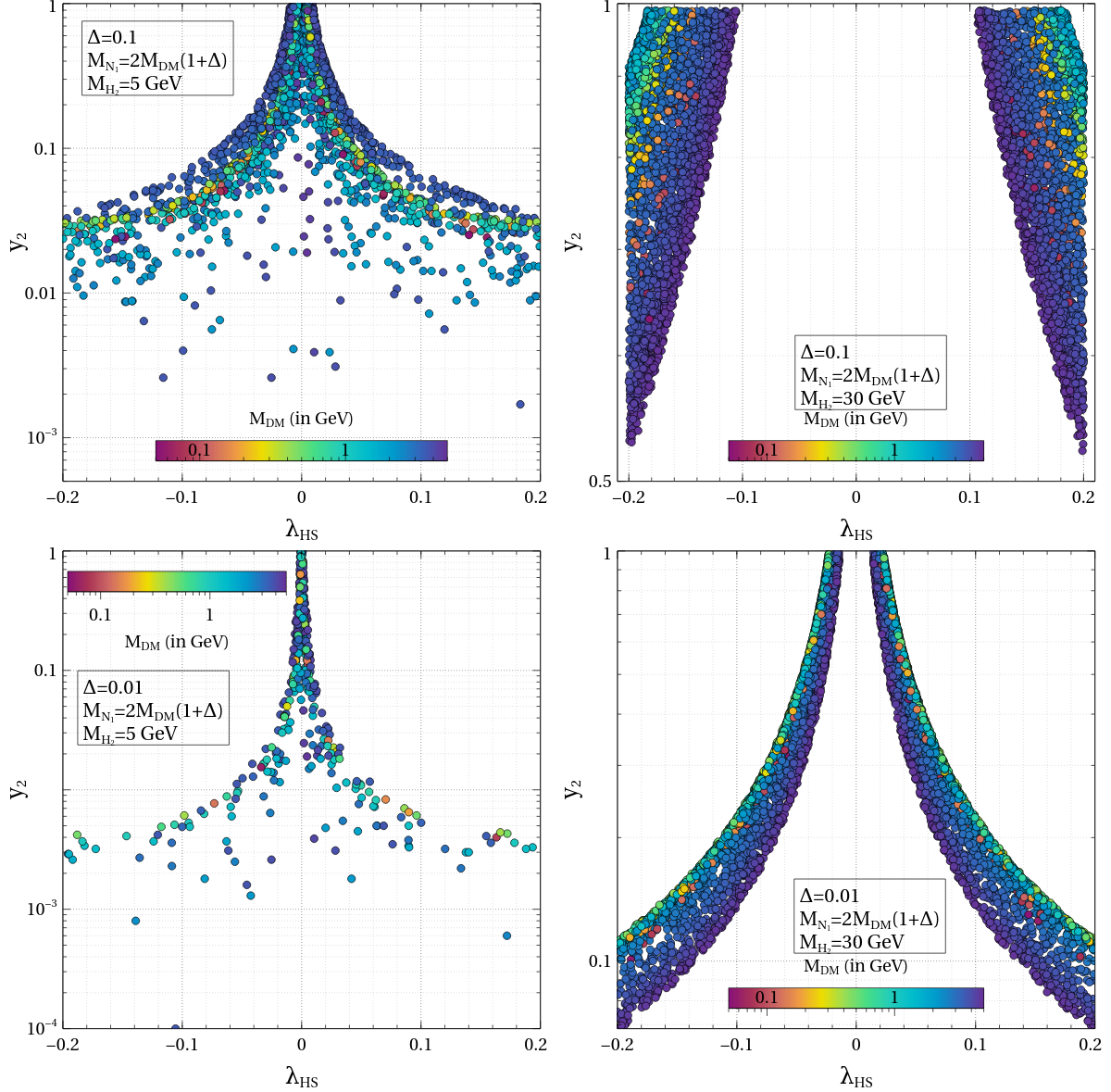


FIG. 7: Allowed parameter space in Higgs portal coupling (λ_{HS}) with the singlet scalar *vs.* the Yukawa coupling (y_2) associated with the second Higgs doublet satisfying the correct relic abundance of DM in the forbidden scenario. The colour bar indicated the dark matter mass in GeV.

by suitably adjusting N_1 mass, DM can also annihilate into $\nu\bar{\nu}$ final states due to mixing of N_1 with active neutrinos by virtue of type-I seesaw. However, due to the chosen values of DM and N_1 mass, such active-sterile mixing remains suppressed leading to negligible contribution from non-forbidden annihilation into light neutrinos. We show this comparison in appendix B.

We also compare the parameter space for forbidden and usual thermal (non-forbidden)

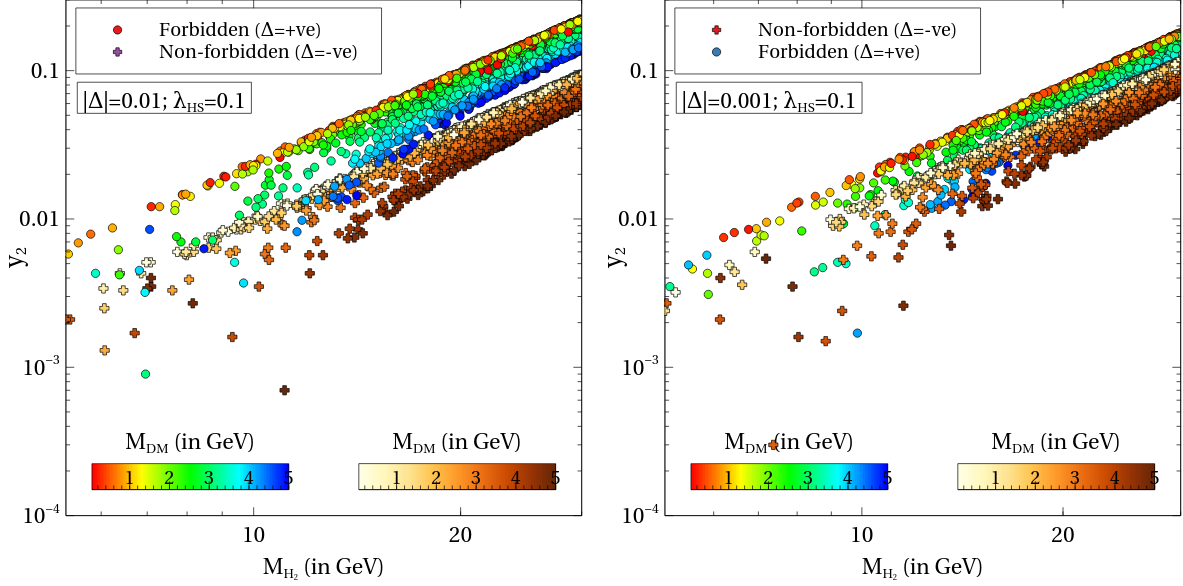


FIG. 8: Comparison between forbidden and non-forbidden allowed parameter space with Yukawa coupling for a fixed Higgs portal coupling λ_{HS} . Correlation with M_{H_2} masses with $\Delta = 0.01$ ($\Delta = 0.001$) are shown in the x-axis and the colour bar stands for the dark matter mass in the left (right) panel. All the points satisfy relic abundance of dark matter at 3σ C.L.

DM from relic abundance criteria. Fig. 8 shows the comparison where the parameter space in y_2 and M_{H_2} plane satisfies the correct DM relic. Clearly, the forbidden scenario corresponds to larger Yukawa couplings in order to get the correct relic. We can see from Fig. 8 that the separation between the allowed parameter space for forbidden DM and non-forbidden DM shrinks for smaller Δ . This is expected as smaller Δ values lead to a smaller Boltzmann suppression, resulting in a larger cross-section. Therefore, to bring the relic density of the DM to the correct ballpark, we need a smaller Yukawa coupling. The circular colour markers represent the forbidden case while the coloured *plus* shaped markers represent the non-forbidden case in both figures. The variations with M_{DM} in each case are shown in the colour bar.

B. The leptophilic ϕ_2

When we opt for the leptophilic scalar doublet ϕ_2 , it brings about substantial changes in the dark matter parameter space compared to the neutrinophilic scenario. This is due to the fact that the final state masses can not be chosen arbitrarily to keep DM in the forbidden

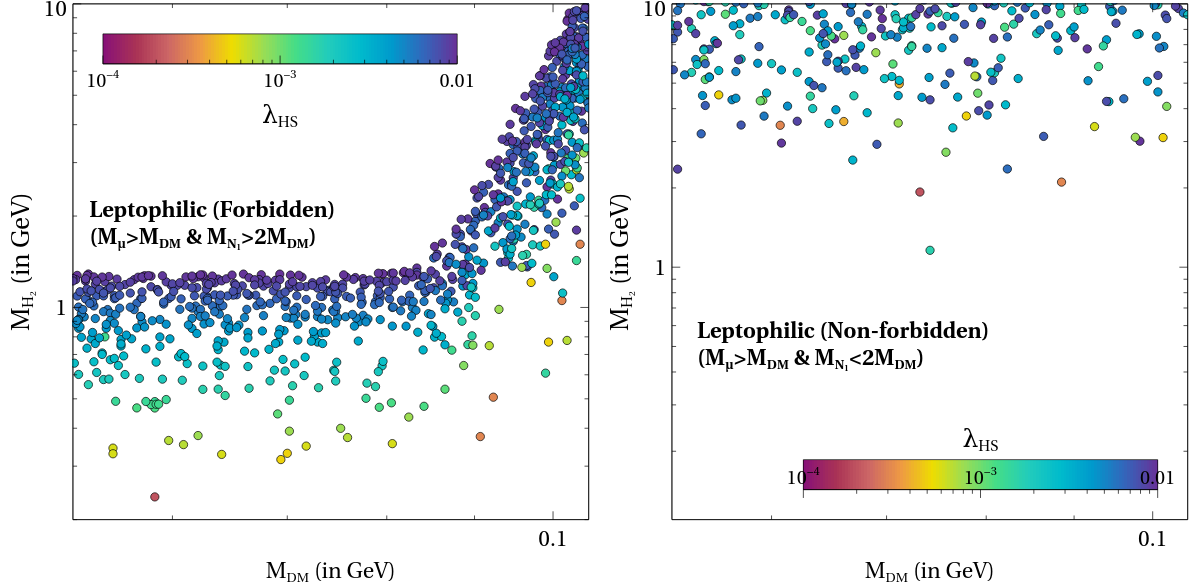


FIG. 9: DM relic satisfied points for the leptophilic case with forbidden (left panel) and non-forbidden (right panel) final states. We show the Higgs portal coupling as the continuous colour spectrum here. As we are concerned with the $(g-2)_\mu$, therefore, in the leptophilic case, we have scanned up to the mass ~ 105 MeV.

ballpark. The significance of the neutrino Yukawa coupling (y_2) diminishes, while the charged lepton Yukawa coupling (Y_2) takes on a more or equally dominant role in determining the relic density. As we consider DM mass range from 50 MeV to a few GeV, we can not keep the e^+e^- final states forbidden, however, we make it suppressed by choosing electron coupling with ϕ_2 to be negligible. We keep a sizeable coupling of the muon with ϕ_2 motivated from $(g-2)_\mu$ and accordingly, keep the $\mu^+\mu^-$ final states in the forbidden ballpark. While our primary goal is to study the forbidden DM case with both $N_1\bar{\nu}_\alpha$ and $\mu^+\mu^-$ final states in the kinematically forbidden ballpark, we also check the corresponding results for the non-forbidden case as a comparison. While we still keep the charged lepton final states suppressed or kinematically forbidden, we kinematically allow the $N_1\bar{\nu}_\alpha$ to go to the non-forbidden regime while still explaining $(g-2)_\mu$ and satisfying CMB bounds on DM annihilation into charged fermion states during recombination.

Fig. 9 shows the parameter space in $M_{H_2} - M_{DM}$ plane and scalar portal coupling λ_{HS} in colour code, for both forbidden and non-forbidden DM with leptophilic ϕ_2 as mediator. The Yukawa coupling Y_2^μ is varied in the ballpark consistent with $(g-2)_\mu$ while Y_2^e, Y_2^τ are

negligible. The choice of y_2 is kept within the interval $[10^{-3}, 10^{-2}]$. As the left panel of Fig. 9 shows, there is an abrupt surge in the required values of M_{H_2} , particularly starting from around $M_{\text{DM}} \sim 90$ MeV. This is because, as DM mass becomes closer to muon mass, the relative mass splitting Δ decreases leading to reduced Boltzmann suppression. If we keep the scalar portal and Yukawa couplings fixed, we need to increase the mass of mediator M_{H_2} to get the correct relic abundance while compensating for the decrease in Boltzmann suppression of final states. Similarly, in the right panel for the non-forbidden case, we observe a push for a larger mediator mass to satisfy the relic density constraint while keeping all other parameters fixed. This is once again due to the requirement of reducing the annihilation cross-section to get the correct relic abundance after Boltzmann suppression in final states disappears. As expected, the non-forbidden process $SS \rightarrow N_1 \bar{\nu}_\alpha$ dominates over the forbidden process $SS \rightarrow \mu^+ \mu^-$ in controlling the relic of the non-forbidden scenario.

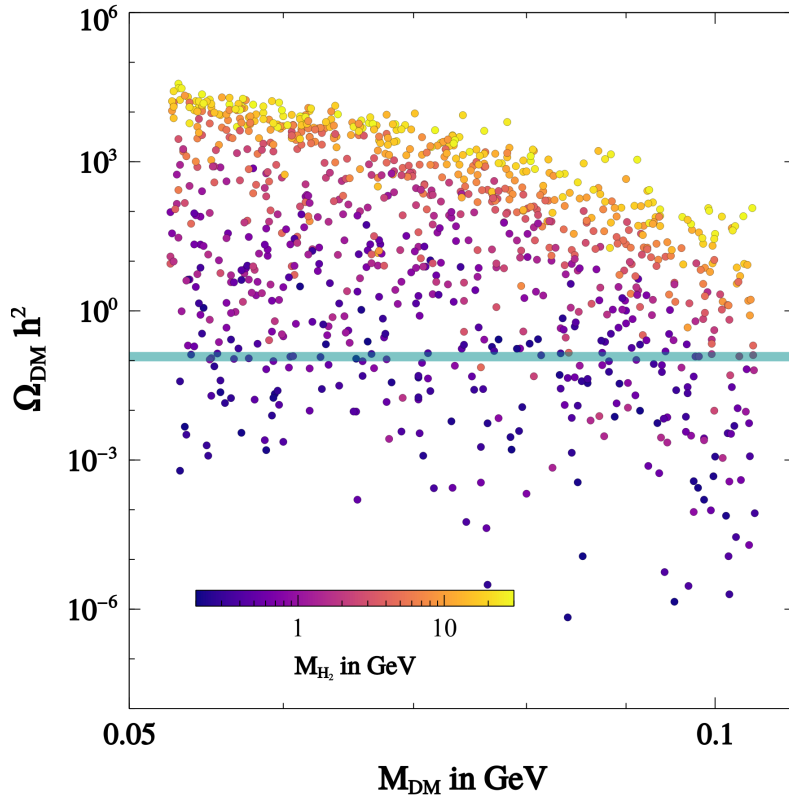


FIG. 10: Relic density as a function of DM mass for the points satisfying constraints from Δa_μ and MEG-I.

Fig. 10 shows DM relic versus DM mass in the leptophilic ϕ_2 case with colour code denoting H_2 mass. The points shown in this figure satisfy the criteria of $(g-2)_\mu$ and LFV

constraints, discussed in section IV. Since the parameters influencing Δa_μ and $\text{BR}(\mu \rightarrow e\gamma)$ are already restricted due to experimental bounds, the other relevant parameter is varied randomly as $\lambda_{HS} \in [0.001, 0.01]$. Evidently, there exists a common parameter space that not only complies with the correct relic density of dark matter but also aligns with the constraints arising from the muon anomalous magnetic moment and LFV.

C. CMB constraints

DM annihilating into charged fermions or photons during the recombination epoch can cause noticeable distortions in the CMB anisotropy spectrum and hence there exist stringent constraints [5, 27, 28], particularly for light thermal DM of the mass range discussed in this work. Kinematically forbidden DM remains safe from such bounds as DM annihilation to charged fermion states are Boltzmann suppressed at low temperatures.

The neutrinophilic scenario discussed here remains completely safe from such CMB bounds as DM annihilates only into forbidden final states $N_1 \bar{\nu}_\alpha$ and even at one-loop level there is no DM annihilation process into photons. However, in the leptophilic case, loop-level annihilation of DM into two photons is still viable and thus imposes a stringent constraint on this annihilation rate during the recombination epoch. Although there is a loop suppression, the final states (photons) are in non-forbidden mode and hence can face tight constraints from CMB.

In Fig. 11, we scrutinize the points satisfying correct relic density as well as $(g - 2)_\mu$ and LFV constraints against the constraint on DM annihilation to photons during the CMB decoupling [28]. The circular colour-coded points, with the colour bar indicating the mass of M_{H_2} , correspond to those depicted in Fig. 9 meeting the correct relic density constraint for DM. The dark cyan star-shaped points align with the correct relic density satisfying points from Fig. 10. Consequently, these points collectively fulfil $(g - 2)_\mu$, LFV constraints, and correct relic density simultaneously. Clearly, there is a viable parameter space that meets all these criteria while remaining consistent with the CMB constraints.

Interestingly, even the non-forbidden DM scenario of the model can be saved from the CMB bounds by appropriately choosing the final states. For example, if DM annihilates dominantly into $N_1 \bar{\nu}_\alpha$, the CMB constraints can be made weaker. At first glance, one might assume that this situation is immune to constraints from CMB considerations. However,

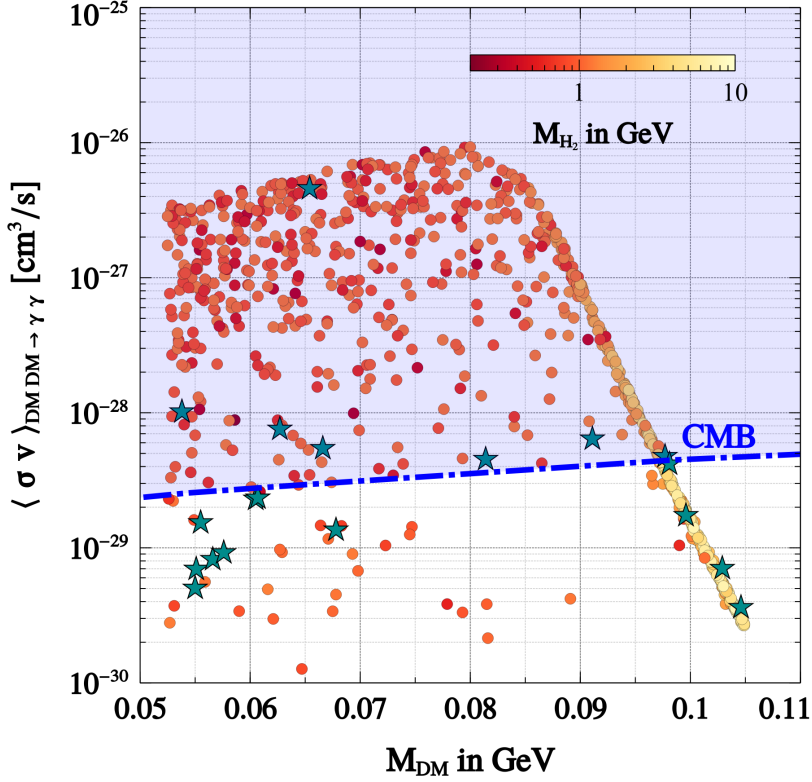


FIG. 11: Points satisfying correct relic density, $(g - 2)_\mu$ and LFV constraints, against the CMB constraints on $\langle \sigma v \rangle_{\text{DM DM} \rightarrow \gamma \gamma}$. The circular colour-coded points satisfy the correct relic density, while the dark cyan star-shaped points fulfil $(g - 2)_\mu$, LFV constraints, and correct relic density simultaneously.

the accessibility of decay channels for N_1 , leading to $\nu e^+ e^-$, introduces potential issues, subjecting it to significant constraints imposed by CMB anisotropy bounds. In our specific configuration, the presence of a light scalar H_2 results in N_1 primarily decaying into 3ν , with its decay into $\nu e^+ e^-$ being effectively suppressed. This suppression arises due to the chosen tiny value of H_2 -electron Yukawa coupling Y_2^e and heavy mediator (SM gauge and Higgs bosons) suppression of $N_1 \rightarrow \nu e^+ e^-$ decay channel. Consequently, the entire parameter space manages to evade constraints imposed by CMB considerations in the non-forbidden case.

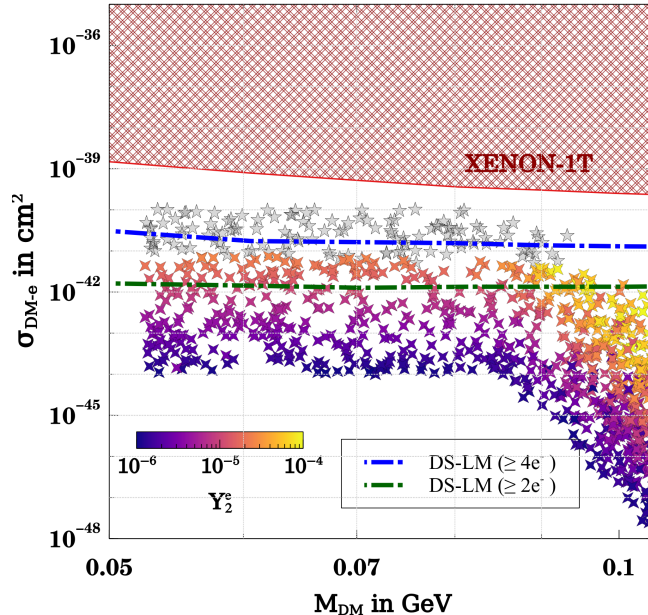


FIG. 12: DM-electron scattering cross-section as a function of DM mass for the points satisfying correct relic density. The colour code depicts the value of Y_2^e coupling. The grey points are ruled out by the CMB constraint on DM annihilation into electrons [5, 28].

D. Direct Detection of DM

In our setup, DM can interact with both nucleons and electrons within terrestrial DM detectors. DM-electron scattering occurs through the H_2 scalar in the leptophilic scenario. However, when the coupling between H_2 and electrons is substantial, it may pose a challenge, conflicting with constraints derived from CMB observations. This is because the same coupling has the potential to enhance the DM annihilation cross-section into electrons.

In Fig. 12, we showcase the DM-electron scattering cross-section as a function of DM mass for the points satisfying correct relic density as shown in Fig. 9. The colour code depicts the value of the coupling Y_2^e which we vary in a range $[10^{-6}, 10^{-4}]$. The grey-coloured points are ruled out by the constraint on DM annihilation to electrons from CMB [5, 28]. We also showcase the most stringent constraints and the on DM-electron scattering cross-section from XENON-1T [64] and the projected sensitivity of DS-LM [65]. The shaded regions depict the constraint from XENON-1T and the dot-dashed lines depict the projected sensitivity of DS-LM.

The DM-nucleon scattering can take place via the SM Higgs mediation. In Fig. 13,

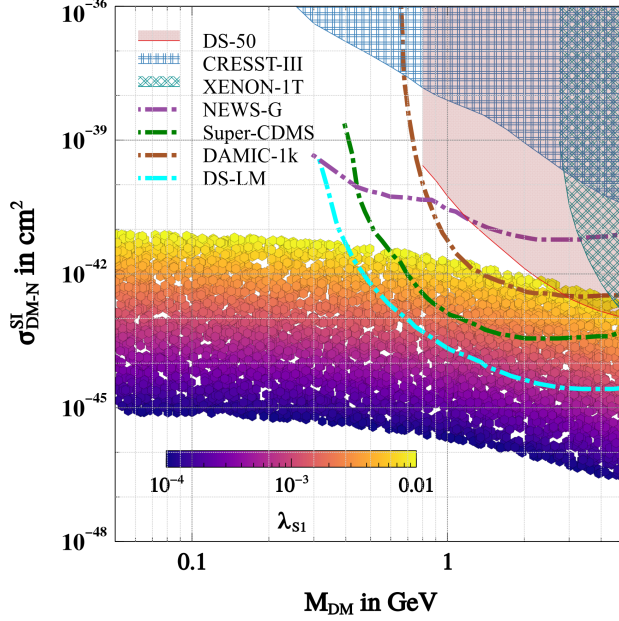


FIG. 13: Spin-independent DM-nucleon scattering as a function of DM with the λ_{S1} coupling shown in the colour code.

we showcase the spin-independent DM-nucleon scattering cross-section as a function of DM mass by varying the coupling λ_{S1} in a range $[10^{-4}, 10^{-2}]$ which is depicted in the colour code. We also project the constraints from XENON-1T [64], CRESST-III [35] and DS-50 [36] by the shaded regions as well as the projected sensitivities of NEWS-G, Super-CDMS [66], DAMIC-1k [67] and DS-LM [65] by the dot-dashed lines. We also check that the chosen values of Y_2^e, λ_{S1} in the direct-detection analysis do not affect the relic abundance of DM.

VII. DETECTION PROSPECTS OF HNL

HNL with masses in the MeV to GeV scale has compelling detection prospects in present and future target experiments as they have been searched for via the signature of kinks in the Kurie plots in nuclear beta decays, via anomalous peaks in the energy spectra of charged leptons in two-body leptonic decays of pseudoscalar mesons and in the apparent deviation of ratio of branching fraction of mesons to leptons from their SM values. For example, HNL can lead to a deviation of the ratio $\text{BR}(K^+ \rightarrow e^+ + \nu_e)/\text{BR}(K^+ \rightarrow \mu^+ + \nu_\mu)$ as well as for the decay of π^+ . Similarly, HNL can be probed in the apparent deviation of the spectral parameters in μ and leptonic τ decay from their SM values. Here it is worth mentioning that

the HNL masses and mixing with distinct neutrino flavours can be considered independent free parameters from a model-independent standpoint. However, generating light neutrino masses imposes theoretical restrictions, creating a link between the HNL and active neutrino sectors that might be used as guidance for future experimental studies.

HNL production and decay in minimal scenarios are governed by SM interactions and the mixing of HNL with the active neutrino, resulting in relatively long lifetimes if the masses are in the MeV-GeV range. This is the foundation of searches, such as those conducted at colliders and beam dump experiments. HNL have new sources of production and decay channels in models with more interactions. If the extra interactions associated with dark matter become stronger, it may increase scattering cross sections and quick decays, fundamentally altering the HNL phenomenology. If it decays promptly into neutrinos or other unseen particles, for example, it can weaken collider and beam dump limitations since the HNL would not have reached the detector, and other signals would have been reduced by the branching ratio into invisible channels. In our scenario, though HNL has additional interaction, if H_2 is heavier than the standard searches for HNL remain valid. However, if H_2 is lighter than HNL, then N_1 will dominantly decay to ν and H_2 and hence all these constraints become irrelevant in that scenario.

In peak search experiments, the best constraints on HNL are from τ lepton and meson decays. Some of the considered meson decays for HNL searches are $\pi^\pm \rightarrow \ell^\pm N_1$, $K^\pm \rightarrow \ell^\pm N_1$, $K^\pm \rightarrow \pi^0 \ell^\pm N_1$, $D^\pm \rightarrow \ell^\pm N_1$, $D_s^\pm \rightarrow \ell^\pm N_1$, $D^+ \rightarrow \ell^+ \bar{K}^0 N_1$ and its conjugate decay and τ lepton decays $\tau \rightarrow \pi N_1$, $\tau \rightarrow \rho N_1$ and $\tau \rightarrow \ell \bar{\nu}_l N_1$. Even higher masses can be probed via B meson decays $B \rightarrow X N_1$, where X are mesons. Similarly, a light HNL can be regarded as a long-lived particle (LLP) in beam dump experiments. Mesons produced during particle accelerator beam collision events can decay to HNL and SM particles. The long-lived HNL can then travel away from the beam collision zone without being affected and decay elsewhere in the detector. At the LHC, HNL can be produced in the GeV mass range through heavy meson decays, τ leptons, W and Z bosons, Higgs bosons, and even top quarks. Above B meson mass, HNL can be investigated in high luminosity LHC (HL-LHC) by searching for displaced vertices. Also, the HNL being lighter than Z boson mass can also be produced by $Z \rightarrow \nu N_1$. This can be probed via a proposed FCC-ee experiment[68].

In Fig. 14, the values of active neutrino-HNL mixing angle θ_{e4} calculated using Casas-Ibarra parameterization in the type-I seesaw scenario (given in Eq. (9)) are shown via

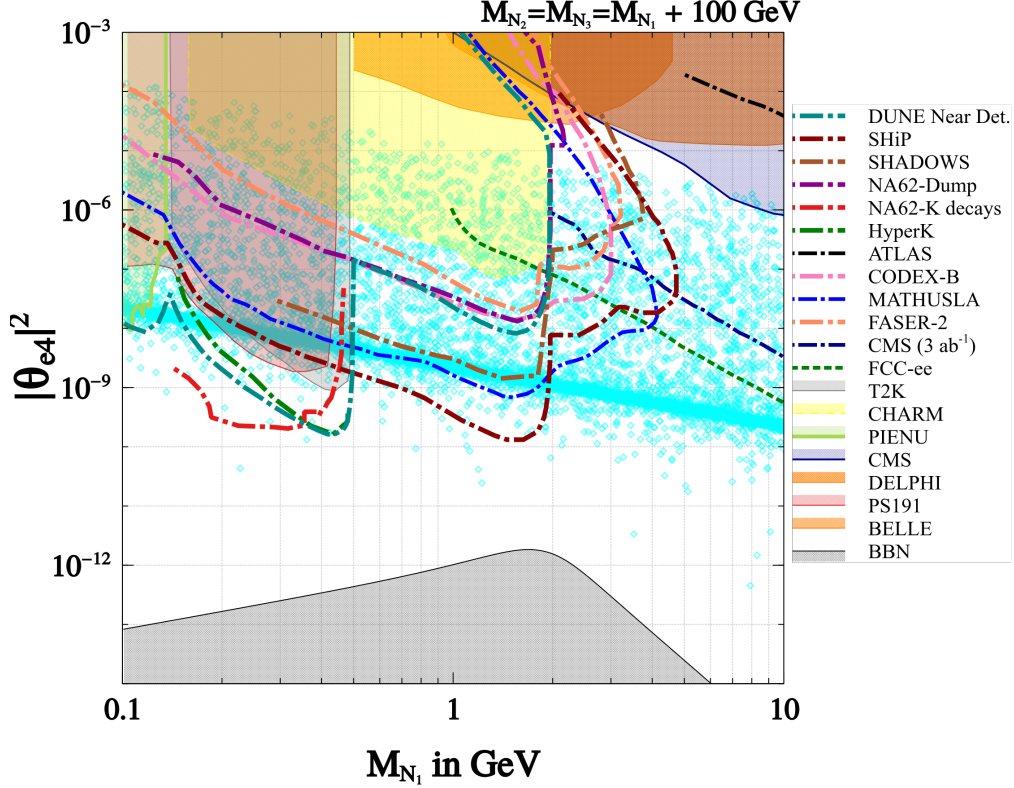


FIG. 14: $|\theta_{e41}|^2$ as a function of M_{N_1} in our setup is shown by the cyan-coloured points. The shaded regions depict the existing constraints and the dot-dashed, dashed lines depict the projected sensitivities of various experiments.

the cyan points where we have imposed the upper limit on absolute neutrino mass from the KATRIN experiment [69]. Existing limits from PS191 [70], CHARM [71], PIENU[72]), NA62[73], T2K[74], Belle[75], DELPHI[76], ATLAS[77], and CMS [78] are shown by differently shaded regions and the projected sensitivities from the NA62- dump[79], NA62 K^+ decays[73], SHADOWS[80], SHiP[81], DUNE near detector[82]),Hyper-K[74], FASER[83], Codex-b[84] and MATHUSLA[85] are shown by the dot dashed or dotted lines, as indicated by the labels. The BBN lower limit on the mixing parameter (or upper limit on HNL lifetime) ensures that HNL decay does not affect the successful BBN predictions. We have considered a viable parameter space for the HNL mass from 100 MeV to 10 GeV from the requirement of achieving correct relic density. Discussions on even lower HNL mass can be found in [61, 62]. To be consistent with the constraints from BBN, we restrict the HNL lifetime to be less than 0.1 s. For this, we take into account all the decay channels of RHN and calculate its total decay width. With an increasing mass of the RHN, new decay channels

open up. Depending on the final state particles, these decay channels can be divided into semileptonic (hadronic) and purely leptonic processes. The details of the lifetime calculation are given in appendix A. We consider $M_{H_2} = 30$ GeV, $\lambda_{HS} = 0.1$ and $y_2^{\alpha 1} = 10^{-3}$ considering ϕ_2 to be neutrinophilic in these calculations. The type-I seesaw is assumed to contribute approximately 50% to light neutrino mass throughout our analysis.

Fig. 15 shows the active neutrino-HNL mixing angle as a function of the lightest active neutrino mass, with the colour code depicting the HNL mass. This is generated by randomly varying the complex orthogonal matrix angles z_{ij} , used in Casas-Ibarra parameterisation (Eq. (9)) in $(0 - 2\pi)$ range for both real and imaginary parts. In addition to cosmological constraints on HNL mentioned above, the light neutrino mass is also constrained by cosmology as well as terrestrial experiments. In addition to existing PLANCK constraints on sum of absolute neutrino mass $\sum_i m_i < 0.12$ eV [5], near future CMB experiments like CMB-S4 [86], galaxy surveys like DESI [87] or Euclid [88] can do further scrutiny. While we show the terrestrial experiment KATRIN bound [69] by the shaded region in Fig. 15, future sensitivity of other laboratory experiments Project 8 [89] is shown as the pink dashed line.

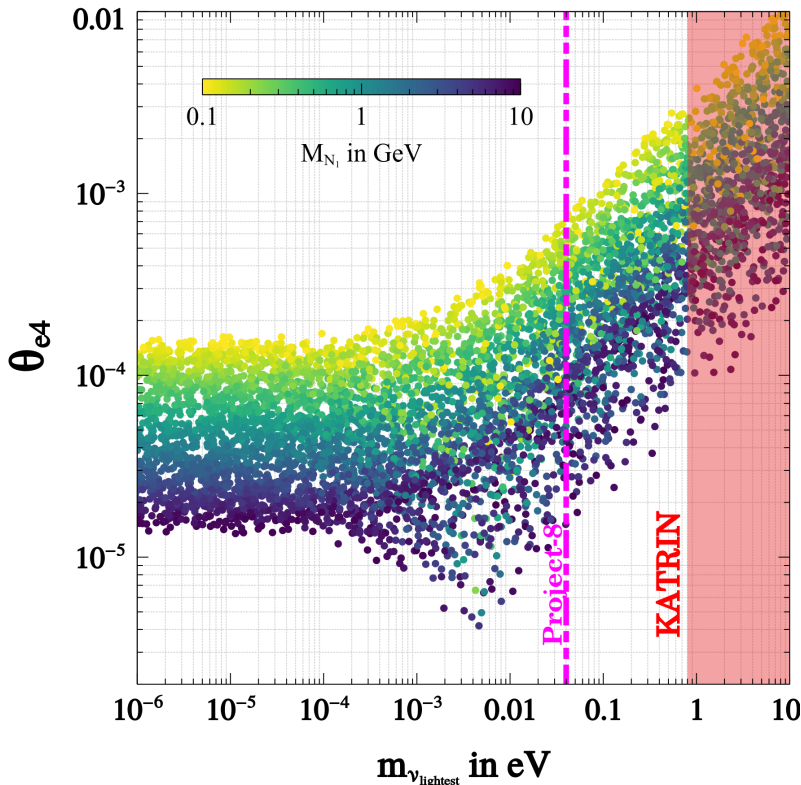


FIG. 15: HNL-SM neutrino mixing angle θ_{e4} as a function of lightest neutrino mass.

VIII. CONCLUSION

We have studied the possibility of light thermal dark matter from sub-GeV to GeV scale by considering a type-I seesaw scenario extended with a second Higgs doublet ϕ_2 . Light DM, assumed to be a real scalar singlet, can have efficient annihilation rates mediated by the neutral component of ϕ_2 , denoted by H_2 . While ϕ_2 does not couple to quarks, it can couple to RHN and SM leptons. We consider the alignment limit where the neutral component of ϕ_2 does not acquire any VEV. However, ϕ_2 coupling with RHN and SM leptons can still give rise to a sizeable contribution to light neutrino masses via the one-loop effect. Depending upon its neutrinophilic or leptophilic nature of H_2 , we study the DM phenomenology by considering equal contribution from tree-level and one-loop seesaw to light neutrino mass.

We study the possibility of kinematically forbidden final states which help in avoiding stringent CMB bounds on light DM annihilation to charged fermion states or photons during recombination. The neutrinophilic scenario is found to be safe from such bounds in both forbidden and non-forbidden modes. The leptophilic scenario, disfavoured in the non-forbidden mode, faces tight constraints in the forbidden mode as well due to the one-loop annihilation rate into photons. Motivated by explaining the anomalous magnetic moment of the muon, we consider muon final states in kinematically forbidden regime in the leptophilic scenario while other charged fermion final states do not arise due to suppressed couplings with ϕ_2 . In the leptophilic scenario, we also show the distinct features in terms of parameter space if we keep the muon final states in the forbidden ballpark while kinematically allowing RHN and SM neutrino final states. The model not only explains muon anomalous magnetic moment and CDF-II W-mass anomaly but can also saturate the charged lepton flavour violation limits. Opening up SM Higgs portal coupling of DM or allowing ϕ_2 coupling to electrons, without contributing significantly to relic while being safe from CMB bounds, can give rise to tree-level direct-detection prospects for DM. This keeps the parameter space within the reach of several direct detection experiments sensitive to light DM. We also discuss the tantalising detection prospects of RHN whose mass remains in the same ballpark as DM mass in order to appear in final states, either in forbidden or non-forbidden mode.

Acknowledgments

The work of DB is supported by the Science and Engineering Research Board (SERB), Government of India grant MTR/2022/000575. PD would like to acknowledge IITG for the financial support under the project grant number: IITG/R&D/IPDF/2021-22/20210911916. SM acknowledges the financial support from the National Research Foundation of Korea grant 2022R1A2C1005050. The work of NS is supported by the Department of Atomic Energy-Board of Research in Nuclear Sciences, Government of India (Ref. Number: 58/14/15/2021- BRNS/37220).

Appendix A: Decay modes of HNL

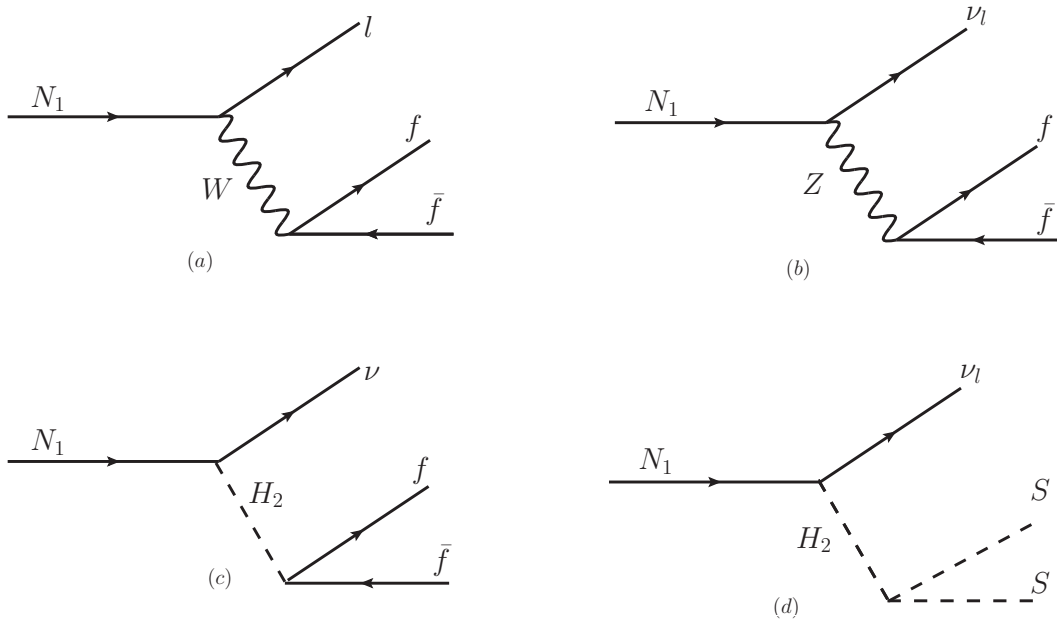


FIG. 16: Two-body and three-body decay modes of HNL, N_1 .

1. Decay into hadrons

In this section, we briefly discuss the decay modes of the heavy Majorana neutrino N_1 , with mass M_{N_1} , much smaller than the mass of the W boson, M_W . The charged current and neutral current vertices of N_1 with the mixing elements are given in Fig. 16. The

decay width scales as the third and the fifth power of the mass(M_{N_1}) for two and three-body decays, respectively.

In this section, we consider hadronic final states for M_{N_1} both below and above Λ_{QCD} scale. The quark pair predominantly binds into a single meson at $M_{N_1} \lesssim \Lambda_{\text{QCD}}$. There are charged current and neutral current mediated processes with a meson in the final state: $N \rightarrow \ell_\alpha h_{P/V}^+$ and $N \rightarrow \nu_\alpha h_{P/V}^0$, where h_P^+ (h_P^0) are charged (neutral) pseudoscalar mesons and h_V^+ (h_V^0) are charged (neutral) vector mesons. In formulas below $x_i \equiv m_i/M_{N_1}$ (with i being the respective particle), f_h and g_h are the corresponding meson decay constants (see [90] for all the numerical values), θ_W is the Weinberg angle. We have considered only those final state particles whose masses are below 10 GeV, such that N_1 decay to them is kinematically allowed. The details of the calculations can be found in [90, 91].

- The decay width to the charged pseudo-scalar (CPS) mesons ($P^+ = \pi^\pm, K^\pm, D^\pm, D_s, B^\pm, B_c$) is given by

$$\Gamma^{CPS} \equiv \Gamma(N \rightarrow \ell_\alpha^- P^+) = \frac{G_F^2 f_P^2 |V_{UD}|^2 |\theta_{\alpha 4}|^2 M_{N_1}^3}{16\pi} \left[(1 - x_\ell^2)^2 - x_P^2 (1 + x_\ell^2) \right] \sqrt{\lambda(1, x_P^2, x_\ell^2)}, \quad (\text{A1})$$

Here λ being the Kallen function [92], defined as:

$$\lambda(x, y, z) = x^2 + y^2 + z^2 - 2xy - 2yz - 2zx. \quad (\text{A2})$$

- The decay width to the neutral pseudo-scalar (NPS) meson ($P^0 = \pi^0, \eta, \eta', \eta_c$) is given by

$$\Gamma^{NPS} \equiv \Gamma(N \rightarrow \nu_\alpha P^0) = \frac{G_F^2 f_P^2 M_{N_1}^3}{32\pi} |\theta_{\alpha 4}|^2 (1 - x_P^2)^2 \quad (\text{A3})$$

- The HNL decay width into charged vector mesons (CVM) ($V^+ = \rho^\pm, a_1^\pm, D_s^{\pm*}, D_s^{\pm*}$) is given by

$$\Gamma^{CVM} \equiv \Gamma(N_1 \rightarrow \ell_\alpha^- V^+) = \frac{G_F^2 g_V^2 |V_{UD}|^2 |\theta_{\alpha 4}|^2 M_{N_1}^3}{16\pi m_V^2} \left((1 - x_\ell^2)^2 + x_V^2 (1 + x_\ell^2) - 2x_V^4 \right) \times \sqrt{\lambda(1, x_V^2, x_\ell^2)} \quad (\text{A4})$$

- For the decay into neutral vector meson (NVM) ($V^0 = \rho^0, a_1^0, \omega, \phi, J/\psi$) we found that the result depends on the quark content of the meson. To consider it, a dimensionless

parameter κ_h is introduced, factor to the meson decay constant [90]. The decay width is given by

$$\Gamma^{NVM} \equiv \Gamma(N_1 \rightarrow \nu_\alpha V^0) = \frac{G_F^2 \kappa_h^2 g_h^2 |\theta_{\alpha 4}|^2 M_{N_1}^3}{32\pi m_V^2} (1 + 2x_V^2) (1 - x_V^2)^2. \quad (\text{A5})$$

- $N_1 \rightarrow \ell_1^- \ell_2^+ \nu_{\ell_2}$ where $\ell_1, \ell_2 = e, \mu, \tau$ with $\ell_1 \neq \ell_2$. This decay mode has charged current interactions only and the decay width is given by

$$\Gamma^{\ell_1 \ell_2 \nu_{\ell_2}} \equiv \Gamma(N_1 \rightarrow \ell_1^- \ell_2^+ \nu_{\ell_2}) = \frac{G_F^2}{192\pi^3} M_{N_1}^5 |\theta_{\alpha 4}|^2 I_1(x_{\ell_1}, x_{\nu_{\ell_2}}, x_{\ell_2}), \quad (\text{A6})$$

$$\text{with } I_1(x, y, z) = 12 \int_{(x+y)^2}^{(1-z)^2} \frac{ds}{s} (s - x^2 - y^2) (1 + z^2 - s) \lambda^{\frac{1}{2}}(s, x^2, y^2) \lambda^{\frac{1}{2}}(1, s, z^2),$$

where $I_1(0, 0, 0) = 1$. We have set the mass of the light neutrino to zero with a very good approximation in the expression for the width above and henceforth.

- $N_1 \rightarrow \nu_{\ell_1} \ell_2^- \ell_2^+$ where $\ell_1, \ell_2 = e, \mu, \tau$. Both charged current and neutral current interactions are relevant for this mode and the decay width is given by

$$\Gamma^{\nu_{\ell_1} \ell_2 \ell_2} \equiv \Gamma(N_1 \rightarrow \nu_{\ell_1} \ell_2^- \ell_2^+) = \frac{G_F^2}{96\pi^3} |\theta_{\alpha 4}|^2 M_{N_1}^5 \times \left[\left(g_L^\ell g_R^\ell + \delta_{\ell_1 \ell_2} g_R^\ell \right) I_2(x_{\nu_{\ell_1}}, x_{\ell_2}, x_{\ell_2}) \right. \\ \left. + \left((g_L^\ell)^2 + (g_R^\ell)^2 + \delta_{\ell_1 \ell_2} (1 + 2g_L^\ell) \right) I_1(x_{\nu_{\ell_1}}, x_{\ell_2}, x_{\ell_2}) \right], \quad (\text{A7})$$

$$\text{with, } I_2(x, y, z) = 24yz \int_{(y+z)^2}^{(1-x)^2} \frac{ds}{s} (1 + x^2 - s) \lambda^{\frac{1}{2}}(s, y^2, z^2) \lambda^{\frac{1}{2}}(1, s, x^2),$$

where $I_2(0, 0, 0) = 1$, $g_L^\ell = -\frac{1}{2} + x_w$, $g_R^\ell = x_w$ and $x_w = \sin^2 \theta_w = 0.231$, where θ_w is the Weinberg angle.

- $N_1 \rightarrow \nu_{\ell_1} \nu \bar{\nu}$ where $\nu_{\ell_1} = \nu_e, \nu_\mu, \nu_\tau$. This decay mode has a neutral current interactions only. Using the massless approximation for the neutrinos as described above the decay width has a simple form given by

$$\Gamma^{3\nu} \equiv \sum_{\ell_2=e}^{\tau} \Gamma(N_1 \rightarrow \nu_{\ell_1} \nu_{\ell_2} \bar{\nu}_{\ell_2}) = \frac{G_F^2}{96\pi^3} |\theta_{\alpha 4}|^2 M_{N_1}^5. \quad (\text{A8})$$

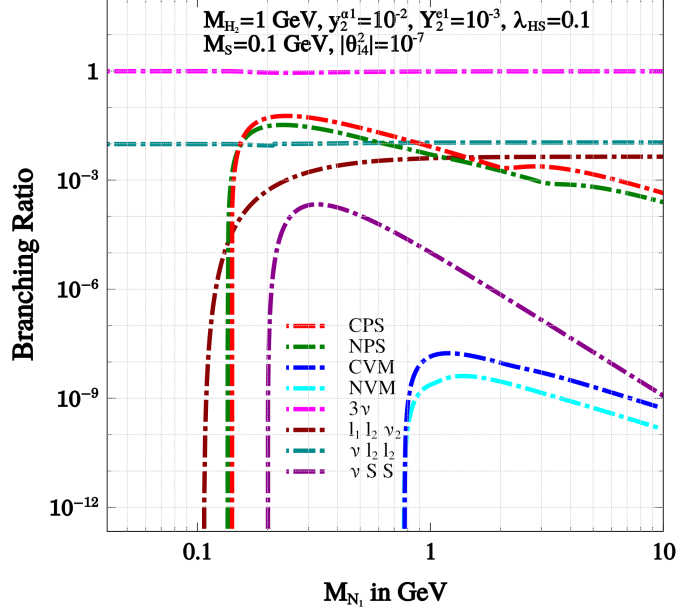


FIG. 17: Branching ratio for various decay modes of HNL (N_1) as a function of N_1 mass are shown for a particular benchmark point.

- H_2 Scalar mediated processes: $N_1 \rightarrow H_2\nu$. The decay width of this tree level decay process, when $M_{N_1} > M_{H_2}$ is given by:

$$\Gamma^{H_2\nu} = \frac{1}{8\pi} y_2^2 M_{N_1}. \quad (\text{A9})$$

The second Higgs-mediated $N_1 \rightarrow 3\nu$ process decay width is given by,

$$\Gamma_{H_2}^{3\nu} = \frac{y_2^2 M_{N_1}^5}{64\pi^3 M_{H_2}^4}, \quad (\text{A10})$$

and for the $N_1 \rightarrow e\nu_2\nu_2$ decay, the decay width is,

$$\Gamma_{H_2}^{e\nu\bar{\nu}} = \frac{y_2^2 (Y_2^{e1})^2 M_{N_1}^5}{64\pi^3 M_{H_2}^4}. \quad (\text{A11})$$

- $N_1 \rightarrow \nu_l SS$ mediated via H_2 , when $M_{N_1} < M_{H_2}$.

$$\Gamma_{H_2}^{\nu_l SS} = \sum_{l=e}^{\tau} \Gamma(N_1 \rightarrow \nu_l SS) = \frac{y_2^2 \lambda_{HS}^2 v^2}{64\pi^3 M_{H_2}^4} |\theta_{l4}|^2 M_{N_1}^5 [I_2(0, x_S, x_S) + 2I_1(0, x_S, x_S)] \quad (\text{A12})$$

All the decay modes listed above contribute to the total decay width of the heavy Majorana neutrino which is given by:

$$\begin{aligned} \Gamma_{N_1}^{\text{Total}} = & \sum_{\ell,P} \Gamma^{CPS} + \sum_{\ell,V} \Gamma^{NPS} + \sum_{\ell,P} 2\Gamma^{CVM} + \sum_{\ell,V} 2\Gamma^{NVM} + \sum_{\ell_1, \ell_2 (\ell_1 \neq \ell_2)} 2\Gamma^{\ell_1 \ell_2 \nu \ell_2} \\ & + \sum_{\ell_1, \ell_2} \Gamma^{\nu \ell_1 \ell_2 \ell_2} + \sum_{\nu \ell_1} \Gamma^{3\nu} + \sum \Gamma_{H_2}^{3\nu} + \sum \Gamma_{H_2}^{e\nu\bar{\nu}} + \sum \Gamma_{H_2}^{\nu_l SS}, \end{aligned} \quad (\text{A13})$$

where $\ell, \ell_1, \ell_2 = e, \mu, \tau$. For a Majorana neutrino, the $\Delta L = 0$ process $N_1 \rightarrow \ell^- P^+$ as well as its charge conjugate $|\Delta L| = 2$ process $N_1 \rightarrow \ell^+ P^-$ are possible and have the same width. Hence the factor of 2 associated with the decay width of this mode in Eq. (A13). Similarly, the $\Delta L = 0$ and its charge conjugate $|\Delta L| = 2$ process are possible for the decay modes $N_1 \rightarrow \ell^- V^+$ and $N_1 \rightarrow \ell_1^- \ell_2^+ \nu_{\ell_2}$ and hence have a factor of 2 associated with their width in Eq. (A13). The branching ratios for different decay modes, for a set of chosen benchmark values, are shown in Fig. 17. Clearly we can see that the $N_1 \rightarrow 3\nu$ decay mode dominates over all other modes. This consequently ensures that our scenario remains safe from CMB constraints.

Appendix B: Comparison of DM annihilation rates

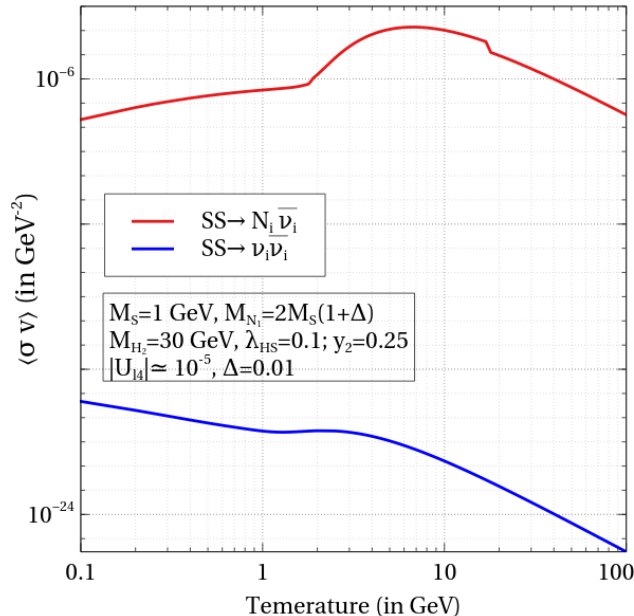


FIG. 18: Comparison of the DM annihilation cross-section with an RH neutrino and an active neutrino in the final state (red) and two neutrinos in the final state (blue). The blue line is heavily suppressed due to the active-sterile mixing element, and thus will not contribute to the DM abundances.

Light thermal DM in the GeV scale keeps annihilating into different final states even after electroweak symmetry breaking (EWSB). Below EWSB, the SM Higgs acquires a VEV leading to mixing between HNL and SM neutrinos. Therefore, even though DM annihilation

into $N_1\bar{\nu}_\alpha$ remains in the forbidden regime, DM annihilation into $\nu\bar{\nu}$ is always allowed and can occur due to $N_1 - \nu$ mixing. Fig. 18 shows the comparison of DM annihilation cross-section to these two final states. As can be seen from the figure, the non-forbidden annihilation into $\nu\bar{\nu}$ final states remains suppressed and negligible compared to that of the forbidden channel. This is due to tiny $N_1 - \nu$ mixing for the chosen N_1 masses required for GeV and sub-GeV scale forbidden DM.

-
- [1] F. Zwicky, *Die Rotverschiebung von extragalaktischen Nebeln*, *Helv. Phys. Acta* **6** (1933) 110–127. [Gen. Rel. Grav.41,207(2009)].
 - [2] V. C. Rubin and W. K. Ford, Jr., *Rotation of the Andromeda Nebula from a Spectroscopic Survey of Emission Regions*, *Astrophys. J.* **159** (1970) 379–403.
 - [3] D. Clowe, M. Bradac, A. H. Gonzalez, M. Markevitch, S. W. Randall, C. Jones, and D. Zaritsky, *A direct empirical proof of the existence of dark matter*, *Astrophys. J.* **648** (2006) L109–L113, [[astro-ph/0608407](#)].
 - [4] **Particle Data Group** Collaboration, P. A. Zyla et al., *Review of Particle Physics*, *PTEP* **2020** (2020), no. 8 083C01.
 - [5] **Planck** Collaboration, N. Aghanim et al., *Planck 2018 results. VI. Cosmological parameters*, *Astron. Astrophys.* **641** (2020) A6, [[arXiv:1807.06209](#)]. [Erratum: *Astron. Astrophys.* 652, C4 (2021)].
 - [6] E. W. Kolb and M. S. Turner, *The Early Universe*, vol. 69. 1990.
 - [7] G. Arcadi, M. Dutra, P. Ghosh, M. Lindner, Y. Mambrini, M. Pierre, S. Profumo, and F. S. Queiroz, *The Waning of the WIMP? A Review of Models, Searches, and Constraints*, [arXiv:1703.07364](#).
 - [8] **LUX-ZEPLIN** Collaboration, J. Aalbers et al., *First Dark Matter Search Results from the LUX-ZEPLIN (LZ) Experiment*, [arXiv:2207.03764](#).
 - [9] B. W. Lee and S. Weinberg, *Cosmological Lower Bound on Heavy Neutrino Masses*, *Phys. Rev. Lett.* **39** (1977) 165–168.
 - [10] E. W. Kolb and K. A. Olive, *The Lee-Weinberg Bound Revisited*, *Phys. Rev. D* **33** (1986) 1202. [Erratum: *Phys. Rev. D* 34, 2531 (1986)].
 - [11] C. Boehm and P. Fayet, *Scalar dark matter candidates*, *Nucl. Phys. B* **683** (2004) 219–263,

- [[hep-ph/0305261](#)].
- [12] M. Pospelov, A. Ritz, and M. B. Voloshin, *Secluded WIMP Dark Matter*, *Phys. Lett. B* **662** (2008) 53–61, [[arXiv:0711.4866](#)].
- [13] R. T. D’Agnolo and J. T. Ruderman, *Light Dark Matter from Forbidden Channels*, *Phys. Rev. Lett.* **115** (2015), no. 6 061301, [[arXiv:1505.07107](#)].
- [14] A. Berlin and N. Blinov, *Thermal Dark Matter Below an MeV*, *Phys. Rev. Lett.* **120** (2018), no. 2 021801, [[arXiv:1706.07046](#)].
- [15] R. T. D’Agnolo, D. Liu, J. T. Ruderman, and P.-J. Wang, *Forbidden dark matter annihilations into Standard Model particles*, *JHEP* **06** (2021) 103, [[arXiv:2012.11766](#)].
- [16] J. Herms, S. Jana, V. P. K., and S. Saad, *Minimal Realization of Light Thermal Dark Matter*, *Phys. Rev. Lett.* **129** (2022), no. 9 091803, [[arXiv:2203.05579](#)].
- [17] C. Jaramillo, *Reviving keV sterile neutrino dark matter*, *JCAP* **10** (2022) 093, [[arXiv:2207.11269](#)].
- [18] D. N. Spergel and P. J. Steinhardt, *Observational evidence for selfinteracting cold dark matter*, *Phys. Rev. Lett.* **84** (2000) 3760–3763, [[astro-ph/9909386](#)].
- [19] S. Tulin and H.-B. Yu, *Dark Matter Self-interactions and Small Scale Structure*, *Phys. Rept.* **730** (2018) 1–57, [[arXiv:1705.02358](#)].
- [20] D. Borah, S. Mahapatra, N. Sahu, and V. S. Thounaojam, *Self-interacting dark matter and the GRB221009A event*, *Phys. Rev. D* **108** (2023), no. 8 083038, [[arXiv:2308.06172](#)].
- [21] D. Borah, S. Mahapatra, and N. Sahu, *New realization of light thermal self-interacting dark matter and detection prospects*, *Phys. Rev. D* **108** (2023), no. 9 L091702, [[arXiv:2211.15703](#)].
- [22] D. Borah, M. Dutta, S. Mahapatra, and N. Sahu, *Boosted Self-Interacting Dark Matter and XENON1T Excess*, [arXiv:2107.13176](#).
- [23] D. Borah, M. Dutta, S. Mahapatra, and N. Sahu, *Self-interacting dark matter via right handed neutrino portal*, *Phys. Rev. D* **105** (2022), no. 1 015004, [[arXiv:2110.00021](#)].
- [24] D. Borah, M. Dutta, S. Mahapatra, and N. Sahu, *Singlet-doublet self-interacting dark matter and radiative neutrino mass*, *Phys. Rev. D* **105** (2022), no. 7 075019, [[arXiv:2112.06847](#)].
- [25] D. Borah, A. Dasgupta, S. Mahapatra, and N. Sahu, *Unified origin of dark matter self interactions and low scale leptogenesis*, *Phys. Rev. D* **106** (2022), no. 9 095028, [[arXiv:2112.14786](#)].
- [26] M. Dutta, N. Narendra, N. Sahu, and S. Shil, *Asymmetric self-interacting dark matter via*

- Dirac leptogenesis*, *Phys. Rev. D* **106** (2022), no. 9 095017, [[arXiv:2202.04704](#)].
- [27] M. S. Madhavacheril, N. Sehgal, and T. R. Slatyer, *Current Dark Matter Annihilation Constraints from CMB and Low-Redshift Data*, *Phys. Rev. D* **89** (2014) 103508, [[arXiv:1310.3815](#)].
- [28] T. R. Slatyer, *Indirect dark matter signatures in the cosmic dark ages. I. Generalizing the bound on s-wave dark matter annihilation from Planck results*, *Phys. Rev. D* **93** (2016), no. 2 023527, [[arXiv:1506.03811](#)].
- [29] K. Griest and D. Seckel, *Three exceptions in the calculation of relic abundances*, *Phys. Rev. D* **43** (1991) 3191–3203.
- [30] P. Minkowski, $\mu \rightarrow e\gamma$ at a Rate of One Out of 10^9 Muon Decays?, *Phys. Lett. B* **67** (1977) 421–428.
- [31] M. Gell-Mann, P. Ramond, and R. Slansky, *Complex Spinors and Unified Theories*, *Conf. Proc. C* **790927** (1979) 315–321, [[arXiv:1306.4669](#)].
- [32] R. N. Mohapatra and G. Senjanovic, *Neutrino Mass and Spontaneous Parity Nonconservation*, *Phys. Rev. Lett.* **44** (1980) 912.
- [33] J. Schechter and J. Valle, *Neutrino Masses in $SU(2) \times U(1)$ Theories*, *Phys. Rev. D* **22** (1980) 2227.
- [34] **CDF** Collaboration, T. Aaltonen et al., *High-precision measurement of the W boson mass with the CDF II detector*, *Science* **376** (2022), no. 6589 170–176.
- [35] **CRESST** Collaboration, A. H. Abdelhameed et al., *First results from the CRESST-III low-mass dark matter program*, *Phys. Rev. D* **100** (2019), no. 10 102002, [[arXiv:1904.00498](#)].
- [36] **DarkSide-50** Collaboration, P. Agnes et al., *Search for low-mass dark matter WIMPs with 12 ton-day exposure of DarkSide-50*, *Phys. Rev. D* **107** (2023), no. 6 063001, [[arXiv:2207.11966](#)].
- [37] **XENON** Collaboration, E. Aprile et al., *First Dark Matter Search with Nuclear Recoils from the XENONnT Experiment*, *Phys. Rev. Lett.* **131** (2023), no. 4 041003, [[arXiv:2303.14729](#)].
- [38] J. Bernon, J. F. Gunion, H. E. Haber, Y. Jiang, and S. Kraml, *Scrutinizing the alignment limit in two-Higgs-doublet models: $m_h=125$ GeV*, *Phys. Rev. D* **92** (2015), no. 7 075004, [[arXiv:1507.00933](#)].
- [39] J. Bernon, J. F. Gunion, H. E. Haber, Y. Jiang, and S. Kraml, *Scrutinizing the alignment limit in two-Higgs-doublet models. II. $m_H=125$ GeV*, *Phys. Rev. D* **93** (2016), no. 3 035027,

- [arXiv:1511.03682].
- [40] K. S. Babu, P. S. B. Dev, S. Jana, and A. Thapa, *Non-Standard Interactions in Radiative Neutrino Mass Models*, *JHEP* **03** (2020) 006, [arXiv:1907.09498].
- [41] H. E. Haber and O. Stål, *New LHC benchmarks for the CP -conserving two-Higgs-doublet model*, *Eur. Phys. J. C* **75** (2015), no. 10 491, [arXiv:1507.04281]. [Erratum: *Eur.Phys.J.C* **76**, 312 (2016)].
- [42] E. Lundstrom, M. Gustafsson, and J. Edsjo, *The Inert Doublet Model and LEP II Limits*, *Phys. Rev.* **D79** (2009) 035013, [arXiv:0810.3924].
- [43] Z.-j. Tao, *Radiative seesaw mechanism at weak scale*, *Phys. Rev. D* **54** (1996) 5693–5697, [hep-ph/9603309].
- [44] E. Ma, *Common origin of neutrino mass, dark matter, and baryogenesis*, *Mod. Phys. Lett.* **A21** (2006) 1777–1782, [hep-ph/0605180].
- [45] M. Drewes, *On the Minimal Mixing of Heavy Neutrinos*, arXiv:1904.11959.
- [46] J. A. Casas and A. Ibarra, *Oscillating neutrinos and $\mu \rightarrow e, \gamma$* , *Nucl. Phys. B* **618** (2001) 171–204, [hep-ph/0103065].
- [47] A. Merle and M. Platscher, *Running of radiative neutrino masses: the scotogenic model — revisited*, *JHEP* **11** (2015) 148, [arXiv:1507.06314].
- [48] I. Esteban, M. C. Gonzalez-Garcia, M. Maltoni, T. Schwetz, and A. Zhou, *The fate of hints: updated global analysis of three-flavor neutrino oscillations*, *JHEP* **09** (2020) 178, [arXiv:2007.14792].
- [49] **Muon g-2** Collaboration, D. P. Aguillard et al., *Measurement of the Positive Muon Anomalous Magnetic Moment to 0.20 ppm*, *Phys. Rev. Lett.* **131** (2023), no. 16 161802, [arXiv:2308.06230].
- [50] S. Borsanyi et al., *Leading hadronic contribution to the muon 2 magnetic moment from lattice QCD*, arXiv:2002.12347.
- [51] F. Jegerlehner and A. Nyffeler, *The Muon g-2*, *Phys. Rept.* **477** (2009) 1–110, [arXiv:0902.3360].
- [52] M. Lindner, M. Platscher, and F. S. Queiroz, *A Call for New Physics : The Muon Anomalous Magnetic Moment and Lepton Flavor Violation*, *Phys. Rept.* **731** (2018) 1–82, [arXiv:1610.06587].
- [53] P. Athron, C. Balázs, D. H. Jacob, W. Kotlarski, D. Stöckinger, and H. Stöckinger-Kim, *New*

- physics explanations of a_μ in light of the FNAL muon $g-2$ measurement*, [arXiv:2104.03691](#).
- [54] P. W. Cattaneo, *A search for $\mu^+ \rightarrow e^+\gamma$ with the first dataset of the MEG II experiment*, [arXiv:2310.12614](#).
- [55] **MEG** Collaboration, A. M. Baldini et al., *Search for the lepton flavour violating decay $\mu^+ \rightarrow e^+\gamma$ with the full dataset of the MEG experiment*, *Eur. Phys. J. C* **76** (2016), no. 8 434, [[arXiv:1605.05081](#)].
- [56] **MEG II** Collaboration, A. M. Baldini et al., *The design of the MEG II experiment*, *Eur. Phys. J. C* **78** (2018), no. 5 380, [[arXiv:1801.04688](#)].
- [57] K. S. Babu, S. Jana, and V. P. K., *Correlating W -Boson Mass Shift with Muon $g-2$ in the Two Higgs Doublet Model*, *Phys. Rev. Lett.* **129** (2022), no. 12 121803, [[arXiv:2204.05303](#)].
- [58] D. Borah, S. Mahapatra, P. K. Paul, and N. Sahu, *Scotogenic $U(1)_{L_\mu-L_\tau}$ origin of $(g-2)_\mu$, W -mass anomaly and 95 GeV excess*, [arXiv:2310.11953](#).
- [59] W. Grimus, L. Lavoura, O. M. Ogreid, and P. Osland, *The Oblique parameters in multi-Higgs-doublet models*, *Nucl. Phys. B* **801** (2008) 81–96, [[arXiv:0802.4353](#)].
- [60] D. Borah, S. Mahapatra, D. Nanda, and N. Sahu, *Type II Dirac seesaw with observable ΔN_{eff} in the light of W -mass anomaly*, *Phys. Lett. B* **833** (2022) 137297, [[arXiv:2204.08266](#)].
- [61] O. Ruchayskiy and A. Ivashko, *Experimental bounds on sterile neutrino mixing angles*, *JHEP* **06** (2012) 100, [[arXiv:1112.3319](#)].
- [62] O. Ruchayskiy and A. Ivashko, *Restrictions on the lifetime of sterile neutrinos from primordial nucleosynthesis*, *JCAP* **10** (2012) 014, [[arXiv:1202.2841](#)].
- [63] G. Bélanger, F. Boudjema, A. Goudelis, A. Pukhov, and B. Zaldivar, *micrOMEGAs5.0 : Freeze-in*, *Comput. Phys. Commun.* **231** (2018) 173–186, [[arXiv:1801.03509](#)].
- [64] **XENON** Collaboration, E. Aprile et al., *Light Dark Matter Search with Ionization Signals in XENON1T*, *Phys. Rev. Lett.* **123** (2019), no. 25 251801, [[arXiv:1907.11485](#)].
- [65] **Global Argon Dark Matter** Collaboration, P. Agnes et al., *Sensitivity projections for a dual-phase argon TPC optimized for light dark matter searches through the ionization channel*, *Phys. Rev. D* **107** (2023), no. 11 112006, [[arXiv:2209.01177](#)].
- [66] **SuperCDMS** Collaboration, R. Agnese et al., *Projected Sensitivity of the SuperCDMS SNOLAB experiment*, *Phys. Rev. D* **95** (2017), no. 8 082002, [[arXiv:1610.00006](#)].
- [67] **DAMIC** Collaboration, A. Aguilar-Arevalo et al., *Constraints on Light Dark Matter Particles Interacting with Electrons from DAMIC at SNOLAB*, *Phys. Rev. Lett.* **123** (2019),

- no. 18 181802, [[arXiv:1907.12628](#)].
- [68] **FCC** Collaboration, A. Abada et al., *FCC-ee: The Lepton Collider: Future Circular Collider Conceptual Design Report Volume 2*, *Eur. Phys. J. ST* **228** (2019), no. 2 261–623.
- [69] **KATRIN** Collaboration, M. Aker et al., *Direct neutrino-mass measurement with sub-electronvolt sensitivity*, *Nature Phys.* **18** (2022), no. 2 160–166, [[arXiv:2105.08533](#)].
- [70] G. Bernardi et al., *FURTHER LIMITS ON HEAVY NEUTRINO COUPLINGS*, *Phys. Lett. B* **203** (1988) 332–334.
- [71] **CHARM** Collaboration, F. Bergsma et al., *A Search for Decays of Heavy Neutrinos in the Mass Range 0.5-GeV to 2.8-GeV*, *Phys. Lett. B* **166** (1986) 473–478.
- [72] **PIENU** Collaboration, A. Aguilar-Arevalo et al., *Improved search for heavy neutrinos in the decay $\pi \rightarrow e\nu$* , *Phys. Rev. D* **97** (2018), no. 7 072012, [[arXiv:1712.03275](#)].
- [73] **NA62** Collaboration, E. Cortina Gil et al., *Search for heavy neutral lepton production in K^+ decays to positrons*, *Phys. Lett. B* **807** (2020) 135599, [[arXiv:2005.09575](#)].
- [74] **T2K** Collaboration, K. Abe et al., *Search for heavy neutrinos with the T2K near detector ND280*, *Phys. Rev. D* **100** (2019), no. 5 052006, [[arXiv:1902.07598](#)].
- [75] **Belle** Collaboration, D. Liventsev et al., *Search for heavy neutrinos at Belle*, *Phys. Rev. D* **87** (2013), no. 7 071102, [[arXiv:1301.1105](#)]. [Erratum: *Phys.Rev.D* 95, 099903 (2017)].
- [76] **DELPHI** Collaboration, P. Abreu et al., *Search for neutral heavy leptons produced in Z decays*, *Z. Phys. C* **74** (1997) 57–71. [Erratum: *Z.Phys.C* 75, 580 (1997)].
- [77] **ATLAS** Collaboration, G. Aad et al., *Search for heavy neutral leptons in decays of W bosons produced in 13 TeV pp collisions using prompt and displaced signatures with the ATLAS detector*, *JHEP* **10** (2019) 265, [[arXiv:1905.09787](#)].
- [78] **CMS** Collaboration, A. Tumasyan et al., *Search for long-lived heavy neutral leptons with displaced vertices in proton-proton collisions at $\sqrt{s} = 13$ TeV*, *JHEP* **07** (2022) 081, [[arXiv:2201.05578](#)].
- [79] J. Beacham et al., *Physics Beyond Colliders at CERN: Beyond the Standard Model Working Group Report*, *J. Phys. G* **47** (2020), no. 1 010501, [[arXiv:1901.09966](#)].
- [80] W. Baldini et al., *SHADOWS (Search for Hidden And Dark Objects With the SPS)*, [[arXiv:2110.08025](#)].
- [81] **SHiP** Collaboration, C. Ahdida et al., *Sensitivity of the SHiP experiment to Heavy Neutral Leptons*, *JHEP* **04** (2019) 077, [[arXiv:1811.00930](#)].

- [82] M. Breitbach, L. Buonocore, C. Frugiuele, J. Kopp, and L. Mittnacht, *Searching for physics beyond the Standard Model in an off-axis DUNE near detector*, *JHEP* **01** (2022) 048, [[arXiv:2102.03383](#)].
- [83] **FASEER** Collaboration, A. Ariga et al., *FASEER's physics reach for long-lived particles*, *Phys. Rev. D* **99** (2019), no. 9 095011, [[arXiv:1811.12522](#)].
- [84] G. Aielli et al., *Expression of interest for the CODEX-b detector*, *Eur. Phys. J. C* **80** (2020), no. 12 1177, [[arXiv:1911.00481](#)].
- [85] D. Curtin et al., *Long-Lived Particles at the Energy Frontier: The MATHUSLA Physics Case*, *Rept. Prog. Phys.* **82** (2019), no. 11 116201, [[arXiv:1806.07396](#)].
- [86] **CMB-S4** Collaboration, K. Abazajian et al., *Snowmass 2021 CMB-S4 White Paper*, [[arXiv:2203.08024](#)].
- [87] **DESI** Collaboration, A. Aghamousa et al., *The DESI Experiment Part I: Science, Targeting, and Survey Design*, [[arXiv:1611.00036](#)].
- [88] B. Audren, J. Lesgourgues, S. Bird, M. G. Haehnelt, and M. Viel, *Neutrino masses and cosmological parameters from a Euclid-like survey: Markov Chain Monte Carlo forecasts including theoretical errors*, *JCAP* **01** (2013) 026, [[arXiv:1210.2194](#)].
- [89] **Project 8** Collaboration, A. Ashtari Esfahani et al., *Determining the neutrino mass with cyclotron radiation emission spectroscopy—Project 8*, *J. Phys. G* **44** (2017), no. 5 054004, [[arXiv:1703.02037](#)].
- [90] K. Bondarenko, A. Boyarsky, D. Gorbunov, and O. Ruchayskiy, *Phenomenology of GeV-scale Heavy Neutral Leptons*, *JHEP* **11** (2018) 032, [[arXiv:1805.08567](#)].
- [91] A. Atre, T. Han, S. Pascoli, and B. Zhang, *The Search for Heavy Majorana Neutrinos*, *JHEP* **05** (2009) 030, [[arXiv:0901.3589](#)].
- [92] G. Källén, *Elementary particle physics*. Addison-Wesley, Reading, MA, 1964.